Determination of the Geophysical Model Function of NSCAT and its corresponding variance by the use of Neural Networks

by

C. MEJIA*, F. BADRAN**, A. BENTAMY***

M. CREPON*, S. THIRIA* and N. TRAN*

· Laboratoire d'Océanographie Dynamique et de Climatologie (LODYC), BC 100,
· Université P. et M. Curie
4 Place Jussieu - 75005 PARIS (FRANCE)

** CEDRIC, Conservatoire National des Arts et Métiers
292 rue Saint Martin - 75003 PARIS (FRANCE)

*** IFREMER, Département d'Océanographie Spatiale (DRO/OS), centre de Brest
BP 70 - 29280 PLOUZANE (FRANCE)

Submitted to JGR December 1998

Abstract

We have computed two Geophysical Model Functions (one for the vertical and one for the horizontal polarization) for the NSCAT scatterometer by using neural networks. These Neural Network Geophysical Model Functions (NN-GMF) were estimated with NSCAT scatterometer sigma-0 measurements collocated with ECMWF analyzed wind vectors during the period 15 January 1997 to 15 April 1997.

We performed a Student t-test showing that the NN-GMFs estimate the NSCAT sigma-0 with a confidence level of 95%. Analysis of the results shows that the mean NSCAT signal depends on the incidence angle, on the wind speed and presents the classical bi-harmonic modulation with respect to the wind azimuth. The NSCAT sigma-0 increases with respect to the wind speed and presents a well marked change at around 7 m/s. The upwind-downwind amplitude is higher for horizontal polarization signal than for vertical polarization indicating that the use of horizontal polarization can give additional information for wind retrieval. Comparison of the sigma-0 computed by the NN-GMFs against the NSCAT measured sigma-0 show a quite low RMS except at low wind speeds.

We also computed two specific neural networks for estimating the variance associated to these GMFs. The variances are analyzed with respect to geophysical parameters. This lead us to compute the geophysical signal to noise ratio, i.e. Kp. The Kp values are quite high at low wind speed and decreases at high wind speed. At constant wind speed, the highest Kp are at cross-wind directions showing that the cross wind values are the most difficult to estimate.

These neural networks can be expressed as analytical functions and Fortran subroutines can be provided.

1. INTRODUCTION

NSCAT is a dual swath, Ku-band, scatterometer which was designed by NASA and constructed under its supervision. The goal was to determine wind vectors over the ocean at global scale with an optimum space and time coverage. NSCAT uses 6 antennae, three for each swath **(Fig. 1).** The two mid antennae operate in a dual polarized mode (vertical and horizontal modes) while the four others operate in a vertical polarized mode only. NSCAT has been flying on the Japanese ADEOS satellite from August 1996 up to first July 1997 and gave a very large and unique data set that allows us to determine wind vectors with global coverage. NSCAT stopped functioning the 1st July 1997 due to a power failure of the ADEOS satellite.

Most of the algorithms which have been proposed to compute the wind vectors from scatterometer measurements are based on the inversion of a Geophysical Model Function (GMF) which is a transfer function giving the scatterometer signal (sigma-0) with respect to the wind vector. The determination of an accurate GMF is then of a fundamental interest. Furthermore the GMFs give useful information on the physical behavior of the scatterometer.

In the present study we determine two GMFs for the NSCAT scatterometer by using Neural Networks (NN-GMF hereinafter), one for vertical polarization denoted NN-GMF-V and one for horizontal denoted NN-GMF-H. As shown in previous works (Woiceshyn *et al* , 1986; Donelan and Pierson, 1987) these GMFs are expected to be different. The neural networks are calibrated using the analyzed wind vectors of the ECMWF meteorological model collocated with NSCAT scatterometer sigma-0 measurements.

Neural networks (NN hereinafter) are relevant statistical methods to extract information from data when physical phenomena are very complicated and cannot be described in terms of theoretically based analysis. NN provide empirical statistical models estimated from observations in form of continuous functions. Furthermore these functions can be analyzed in order to get information about the physical phenomena we study.

The layout of this paper is articulated as follows : in Section 2 we present the geophysical problem. In Section 3 we briefly introduce the NN methodology. The data set used for calibration and validation is described in Section 4. The results are analyzed in Section 5. The variance and the error bars of the NN-GMFs are presented in Section 6. A discussion and conclusion make up Section 7.

2. THE GEOPHYSICAL PROBLEM

Scatterometers are active microwave radars which accurately measure the power of the back scattered signal versus incident signal in order to calculate the normalized radar cross section (sigma-0) of the ocean surface. To first order the sigma-0 depends on the sea roughness which is related to the wind speed v, on the azimuth angle χ (which is the horizontal angle between the wind and the antenna beam of the radar) and the incidence angle θ (which is the angle between the radar beam and the vertical at the illuminated cell) (see **Figure 2)**. Other parameters such as the wave height, the wave direction [Donelan and Pierson, 1987; Donelan, 1990; Donelan *et al.,* 1993; Janssen and Woiceshyn, 1992; Nghiem *et al.,* 1993], rain and sea surface temperature [Donelan and Pierson, 1987; Kahma and Donelan, 1993] are also thought to play some role. These parameters which are thought to act at second order will not be taken into account in the determination of the present GMFs.

There are two different approaches to developing a GMF, the theoretical and the empirical one. The theoretical approach deals with hydrodynamic description of the air/sea interface which specifies the relation between wind and sea surface geometry and expresses the electromagnetic back scattering from the rough air/sea interface [Plant, 1986; Donelan and Pierson, 1987; Chen *et al.,* 1992; Weissman *et al.*, 1994]. This leads to very difficult physical and mathematical descriptions since the physics of the above interactions is insufficiently known to allow the construction of theoretically-based geophysical model functions. The empirical approach has thus been widely used. The aim is to statistically reproduce the relation between the sigma-0 measurements and the wind vectors. The methodology is based

on collocations between NSCAT sigma-0 and wind measurements. The accuracy of the GMF is then related to the number of such collocations and the quality of the collocated data set. Since the GMF depends on three parameters which are the incidence angle, wind speed and wind azimuth, an accurate GMF estimation requires a large number of data. Unfortunately the number of collocations of sigma-0 with wind vector measurements obtained at sea with anemometers fixed on buoys is rather small. An alternative is to use winds obtained from Numerical Weather Prediction models (NWP) which yields a large number of synoptic winds. As shown by Liu and Pierson [1994] the use of NWP can introduce systematic biases in the determination of the GMF owing to the discrepancies existing between NWP winds and actual winds. The quality of most of NWP has dramatically improved during the past few years reducing this potential error (Courtier et al, 1998; Andersson et al, 1998). Besides as mentioned in Stoffelen (1998) NWP models provide a wind estimate at a scale of the order of 100 km which is comparable to the footprint of the scatterometer which is 50 km. These winds are spatial averages contrary to measurements taken by anemometers fixed on buoys which are very local and have provided good estimates of the ESA GMF (CMOD4) and IFREMER GMF (Stoffelen and Anderson, 1998b; Rufenach, 1998).

We now present the NN-GMF-V and NN-GMF-H for the NSCAT scatterometer. We follow the procedure described in Mejia et al. [1998] to compute the ERS1 scatterometer GMF (NN-ERS1-GMF hereinafter).

3. DETERMINATION OF THE NSCAT NN-GMFs

Since the NSCAT and ERS1 scatterometers are quite similar, we determine the two NSCAT GMFs using the same methodology as was chosen for determining the GMF of ERS1 [Mejia *et al*., 1998]. Since we assumed that the scatterometer response is a continuous function with respect to θ, χ and v, which is a weak constraint, the computed NN-GMFs can be modeled by Multi-Layer Perceptrons (MLP hereinafter) whose inputs are the above variables. Preliminary results using NSCAT data suggest that the architecture of the MLP

used for NN-ERS1-GMF is adapted but can be somewhat improved by increasing the number of the hidden layers of the NSCAT NN-GMFs. This is justified by the fact that the NSCAT GMF is more complicated than this of ERS1/2 due to its higher RMS error (as it is shown later) and needs more parameters (each weight of the MLP being considered as a parameter of the GMF). Besides NSCAT is more sensitive to external parameters (rain,.....) than ERS1 which is seen in the larger NSCAT Root Mean Square error (RMS, see Section 5). As in all previous scatterometer GMF determinations (Long 1985, Bentamy et al. 1994, Stoffelen and Anderson 1997a,b), the inputs are the wind speed, the wind azimuth and the incidence angle. The architectures of NN-GMF-H and NN-GMF-V are very similar; they have an input layer of 4 neurons corresponding to ν, $sin\ \chi$, $cos\ \chi$ and $sin\ \theta$ **,** and an output layer of a unique linear neuron which gives the estimate of the required sigma-0 measurement. Both NN have two hidden layers but with different numbers of neurons on each layer as found by an optimal determination of the architectures. For NN-GMF-V we used eight neurons on the first hidden layer and six in the second, and for NN-GMF-H we used five neurons on the first hidden layer and four in the second. These architectures are presented in **Figure 3a** and **3b**. NN-GMF-V and NN-GMF-H are made of 86 and 44 parameters respectively which have to be estimated from the data. This estimation is made during an optimization phase by using a training data set dedicated to each polarization and an appropriate cost function. As the cost function plays an important role in the minimization, let us focus interest on it. If it is assumed that:

1) For each observation *i*, the observed sigma-0 , σ_i^0, can be decomposed in the following manner:

$$\sigma_i^o = \sigma_i^{o*} + e_i \qquad (1)$$

where σ_i^{o*} is the mean expected value with respect to the wind vector and e_i is a gaussian noise with zero mean and of variance $Var(e_i)$. The variance $Var(e_i)$ takes into account the geophysical noise which depends on the wind vector, the incidence angle θ and the σ_i^{o*}.

2) The observations of the learning set $(\vec{v}_i, \sigma_i)$ are chosen independently.

3) The NN-GMFs are well parameterized, i.e. there is no over-training and the neural network output s_i is such that that $\sigma_i^{0*} \approx s_i$ [Bishop, 1995]

It then becomes possible to estimate the a-posteriori probability *P(D/W)* of the mean of the observation set *D* constrained by the model which is represented by the weights W_{ij} of the neural network. The associated log likelihood equation is then:

$$L(W) = -Ln\left[P(D/W)\right] = \frac{1}{2}\sum_i \left\{ \frac{\left(s_i - \sigma_i^0\right)^2}{Var(e_i)} + Ln\left(Var(e_i).2\pi\right) \right\} \quad (2)$$

Under the hypotheses 1, 2 and 3, it can be shown that maximizing *P(D/W)* is equivalent to minimizing the log likelihood equation (2).

Hypotheses 2 and 3 can always be verified. If hypothesis 1 is assumed, equation (2) is the log likelihood and can be taken as a cost function in the computation of the weights of the neural network. Equation (2) is minimized using the W_{ij} (the weights of the neural network) as control parameters [Bishop, 1995].

From a practical point of view, a crucial problem remains which is to correctly estimate $Var(e_i)$. Several approximators have been proposed. Among them we can mention the widely used empirical relationship of the form $Var(e_i) = (K_p\ \sigma^0)^2$ where the signal to noise ratio (the so-called K_p) is a constant chosen to be equal to 0.1 [Stoffelen and Anderson, 1997b]. Besides more sophisticated expression have been proposed (Fisher, 1972, Chi *et al*, 1986, Pierson, 1989) where the sigma-0 distribution is Gaussian with a mean equal to σ_i^{o*} and a variance of the form:

$$Var(\sigma_i^0) = \alpha\left(\sigma_i^{0*}\right)^2 + \beta\sigma_i^{0*} + \gamma \quad (3)$$

where the coefficients α, β and γ are dependent on the radar design and the measurement signal to noise ratio.

The obtained performances of a MLP or any statistical estimator strongly depend on the input parameters and their coding. In order to limit the strong non-linearity of the signal and owing to the large dynamical range of the sigma-0 values which is of several orders of magnitude, we decided to code the sigma-0 in dB as argued by Stoffelen and Anderson [1997a]. Since we work in the dB space, the noise of sigma-0 expressed in dB is not any more Gaussian [Stoffelen and Anderson 1997b; Rufenach, 1998] and equation (2) does not represent the log likelihood function associated to *P*.

Consequently in a first approach we determine the weighs of the NN-GMFs using a quadratic cost function of the form:

$$C(W) = \sum_i \left(s_i^d - \sigma_i^{d0} \right)^2 \tag{4}$$

where $s^d{}_i$ represents the output computed by the MLP and σ_i^{d0} the desired output provided by the corresponding data set expressed in dB, the summation being taken over the training set. This cost function has been widely used in neural networks methodology ; it has been shown (Richard and Lipman, 1991) that it gives the a-posteriori probability *P(D/W)* of the mean of the observation set. Besides, it is noticed that the cost function (4) would correspond to the log likelihood criteria if the noise e_i were Gaussian with a constant variance. The quadratic cost function *C(W)* has been shown to be efficient in determining the ERS1 NN GMF (Mejia et al, 1998). The efficiency of this simplified cost function can be improved by using a specific data set for training as explained in the following section.

We will use the log likelihood approach in section 6 in order to determine $Var(e_i)$ when the sigma-0 are estimated in linear scale.

4. THE DATA SET

As already mentioned, the NN-GMFs were computed by using ECMWF analyzed wind

vectors collocated with NSCAT recalibrated sigma-0 from December 1996 to May 1997 onto the North Atlantic Ocean **(latitude** [60N, 20 N]**, longitude** [100W, 5W]**).** We used the observed sigma-0 provided by the six antennae for vertical polarization and for the two antennae for the horizontal polarization. The ECMWF North Atlantic Ocean winds are thought to be of good quality owing to the relatively large number of observations, which are assimilated in the model. Since January 1996, the ECMWF model has also been assimilating ERS1/2 scatterometer winds (Courtier et al, 1998; Andersson et al, 1998), which improves the quality of the ECMWF wind product and reduces the wind error. This error which play a role in the NSCAT GMF determination (Stoffelen and Anderson, 1997b) can be introduced in the cost function by using the covariance matrix of the ECMWF model. But it is difficult to get a simplified accurate estimate of this covariance matrix (Courtier et al, 1998). This error will not be taken explicitly into account in the present simulation which can be justified by the good quality of the ECMWF wind product during the period under study.

The ECMWF wind components are linearly interpolated to the sigma-0 measurement locations. The collocation was processed by the CERSAT-IFREMER. As found in a preliminary work [Mejia *et al*., 1997] the different antennas of the two swaths have the same characteristics; we thus decided to compute a unique GMF for each polarization. The overall data set used consists of 10 millions of collocations representing the four sigma-0s and their related incidence angle. From this data set we randomly extracted 265000 collocated data where we tried to equally represent all speeds and directions at each incidence angle in order to get a statistically representative data set without bias. However the number of data with wind speeds higher than 25 ms^{-1} is small, and wind speed values higher than 30 ms^{-1} are absent. As the ECMWF winds are noisy at low speed and the corresponding NSCAT small sigma-0 too, we decided to cut the different data set at $2ms^{-1}$. The valid range of wind speed is thus [2 ms^{-1}, 25 ms^{-1}]. This set was used in order to make the calibration (training phase in NN dialect). This equalized training data set partially compensates the use of the simplified cost function (2). An independent test set of 1800000 collocated data was used for estimating the performances of the NN-GMFs.

5. ANALYSIS OF NN-GMF-V AND NN-GMF-H

We first tested the validity of the assumptions we made in section 3 in performing a test hypothesis checking the ability of the NN-GMFs to estimate the conditional mean of the sigma-0.

For each incidence angle, the ECMWF wind vectors collocated with the observed sigma-0 are partitioned in 37×7 bins of azimuth angle of 10 ° and wind speed of 3 ms^{-1} each. The wind speed ranges between 3 and 24 ms^{-1}. In each bin *j*, we assumed that the observed sigma-0s (in linear scale) define a sample of a normal distribution *N(*μ, *SD)* where μ is the mean and *SD* the standard deviation (hypothesis 1 and equation 1 in section 3). This hypothesis is reasonable as found on the sigma-0 histogram in each bin (not shown). For each sample we computed the empirical mean $\hat{\mu}_j = \frac{1}{k}\sum_i \sigma_i^0$ and its empirical standard deviation $\hat{SD}$ which is of the form $\hat{SD_j}^2 = \frac{1}{k-1}\sum_i \left(\sigma_i^0 - \mu_j\right)^2$ where *k* is the number of observed sigma-0 in the bin *j*.

For each bin *j*, we have computed the sigma-0 corresponding to the wind vector $\vec{v}$ at the center of the bin by using the NN-GMF. Let us denote s_j this value in linear scale. We tested the hypothesis that s_j represents an estimate of μ_j at a confidence level of 95%. In order to check this, we performed a Student t-test with a significance level α=5% (Kreyzig , 1979) where μ_j is approximated by $\hat{\mu}_j$. **Figure 4** presents the results of the Student t-test for wind speed between 3m/s and 24m/s at different incidence angles ; the white dots indicating the sample (wind speed and wind direction) where the hypothesis is accepted. The results show that the NN-GMFs estimate the mean value of the sigma-0 with a probability of 95% in most cases.

We then performed several statistical tests in order to check the consistency of NN-GMFs. **Table 1a,b** present the BIAS and the RMS (see Annex for definition) for NN-GMF-V and NN-GMF-H with respect to the incidence angle. We have computed these statistic estimators on the test set for the wind speed ranging from 2 ms^{-1} to 24 ms^{-1}. Clearly these results show

the consistency of the two NN-GMFs over the whole swath whatever the incidence angle. As seen in **Table 1,** the BIAS is small (less than 0.3 dB) except at low wind speeds where it can reach 1dB; the RMS. is of the order of 1 dB except at low wind speeds where it can reach up to 5.6 dB. This phenomena can be seen in **Figure 5** and **Figure 6** where we present the scatter-plots of the NN-GMF-V and NN-GMF-H computed sigma-0 against the observed NSCAT sigma-0 at three different incidence angles (θ = 22.2°, 36.1°, 49.4°). These scatter-plots are centered on the diagonal except at very low values of sigma-0 where we observe the inability of the NN-GMFs to generate low sigma-0 values. An explanation could be the fact that ECMWF winds are noisy at low wind speeds. Both training and test sets were cut at wind speeds less than 2 ms^{-1}. At 2 ms^{-1} the NN-GMFs still provide a good estimate of the sigma-0 which is a mean sigma-0 corresponding to a mean wind speed of 2 ms^{-1}. Due to noise some ECMWF 2 ms^{-1} wind speed correspond to actual wind speeds less than 2 ms^{-1}. Their corresponding sigma-0s are thus smaller than those given by the NN-GMFs at a wind speed of 2 ms^{-1}, explaining the apparent over estimation of NN-GMFs at small sigma-0 values in the scatter plots. As evidenced in the contours, few measurements at low wind speed exhibit this drawback when compared with the all the data involved in these comparisons. A method to partially overcome this problem would be to build GMF forced by the wind components as mentioned in Stoffelen and Anderson (1997b).

Let us now analyze the physical behavior of the two NN-GMFs. NN-GMF-V and NN-GMF-H are presented in **Figure 7** and **Figure 8** respectively. These figures display the variations of the two NN-GMFs with respect to the wind azimuth for different wind speeds and at three different incidence angles (22.2°, 36.5°, 49.6°). The NN-GMFs exhibit the classical bi-harmonic modulation with respect to the wind azimuth. As mentioned before this modulation is not imposed a-priori by using a Fourier series decomposition, but result from the neural estimation. At a given wind speed and incidence angle, these curves can be approximated by a Fourier series decomposition of the form:

$$\sigma^0 = A_0\left[1 + A_1\cos\chi + A_2\cos 2\chi\right] \qquad (5)$$

where the coefficient A_0 corresponds to the mean value of the sigma-0 with respect to the

wind azimuth χ, A_1 is related to the upwind/downwind modulation, A_2 to the biharmonic character of the GMF with respect to χ. The coefficients A_n (n = 0, 1, 2) are complex functions with respect to the incidence angle, the wind speed and the polarization.

The up-wind and down wind of the NN-GMFs are at 0° and 180°as in (5) . The two minima may slightly differ from 90° and 270° and may not be of the same value. This slight difference is due to the fact that we do not impose the location of these minima *a priori*. A similar behavior was found on ERS1 NN-GMF (Mejia *et al* , 1998) and a sensitivity study on model noise showed that the larger model error bars of the ERS1 NN-GMF were at cross wind values. Thus we think that the slight variation in cross wind position is more related to statistical estimation rather than a geophysical phenomena. A similar behavior was found in Weisman *et al* (1994). Besides it should be noticed that the minimum of the Fourier expansion of the form (5) are not exactly at. 90°and 270°. For example if A1/A2 = 0.2, the two minimum are located at : 93° and 267°.

Figures 9a, b display the mean value (in dB) with respect to the wind speed (coefficient $A_0(\theta,v)$ of the Fourier decomposition (5)) at different incidence angles for the NN-GMF-V and NN-GMF-H respectively. **Figures 10a, b** display these mean values with respect to incidence angle at different wind speeds. As expected, these curves which represent the graph of $A_0(\theta,v)$ with respect to v and θ are smooth showing the ability of NN methodology to estimate continuous functions from discrete (the incidence angles are quite discrete) and noisy data sets. These mean values decrease with respect to the incidence angle. It is seen that the dynamical range of the mean value of NN-GMF-H is larger than that of NN-GMF-V. For both NN-GMFs the slope of the mean value with respect to the wind speed, which is quite large at moderate wind speed (less than $7ms^{-1}$), reduces at higher wind speeds. This slope change with the wind regime was found in Donelan and Pierson (1987) and observed by Bliven *et al*., [1993] in wave tank experiments.

Figures 11a, b display the upwind minus downwind values (coefficient $A_1(\theta,v)$) with respect to the wind speed at different incidence angles for the NN-GMF-V and NN-GMF-H

respectively. They are expressed in linear scale. The up-wind minus downwind values are larger for NN-GMF-H than for NN-GMF-V, suggesting the horizontal polarization sigma-0 is important in the wind retrieval procedure. At small incidence angles these values can be negative which means that the down wind value can be larger than the up wind one.

Figures 12a, b display the upwind minus crosswind values (coefficient $A_2(\theta,v)$) with respect to the wind speed at different incidence angles for the NN-GMF-V and NN-GMF-H respectively. These values are in linear scale. As they are quite large, the most probable wind directions might be obtained quite easily in the wind retrieval procedure.

The coefficients A1 and A2 are shown in table 2 for different wind speeds and different incidence angles. They are larger than those of ERS1 (Mejia *et al*, 1998) showing a benefit of using the Ku band (NSCAT) rather than the C band (ERS1) for scatterometer.

Figure 13 displays a V-H-V NSCAT cone in a three-dimensional sigma-0 space corresponding to the sigma-0 observed at the same wind cell by the three antennas for incidence angles of 27°, 22° and 27° respectively. In this figure, the mid antenna sigma-0 corresponds to the horizontal polarization sigma-0 in order to benefit of the large values of the upwind minus downwind signal which enhances the separation of the two surfaces of the cone. Note the strong non-linearity of the GMFs which is noticeable on the curvature of the generatrix of the cone (a displacement along the generatrix corresponds to a change in the wind speed) and to the variation of the position of the two surfaces with respect to each other at different incidence angles. When compared to the ERS1 cone given in Mejia *et al* . [1998], the NSCAT cone is flatter which is due to the arrangement of the NSCAT antennae which are asymmetric (**Fig. 1**).

A global comprehension of the physics of the scatterometer can be viewed by drawing a projection of the NSCAT cone like surface onto planes perpendicular to the generatix against the data as done for ERS-1 by Stoffelen and Anderson (1997a). The problem is more complicated than for ERS-1 since the NSCAT cone like surface is a surface in a four dimensional space (the three vertical polarization sigma-0s and the horizontal one). In **Fig 14**

we have drawn a simplified projection of the NSCAT cone in the V-V-H-V space against the data corresponding to a wind speed of 8 ms^{-1} and incidence angles of 27°, 22°, 22° and 27. It is seen that the NN-GMF cone correctly fits the data. Other plane sections have been drawn showing similar results (not shown).

6. DETERMINATION OF THE SIGNAL ERROR BARS

The NN-GMFs have been determined under the assumption (see section 3) that each observation σ^0_i is the sum of the true signal ,σ^o_j* , and a Gaussian noise, e_i , with zero mean and whose variance $Var(e_i)$ is constant.

As shown in Section 5 the two NSCAT NN-GMFs accurately estimate the corresponding σ^o_j*. The second assumption (constant variance) is a rough approximation of the reality. Besides the knowledge of $Var(e_i)$ gives useful information on the response of the scatterometer and the accuracy of the NN-GMFs. In the following we relax the above assumption and estimate $Var(e_i)$.

We assume that the variance of the observed sigma-0 is a function of the true sigma-0 (σ^o_j*), of the wind vector $\vec{v}$ and of the incidence angle θ. We estimate the conditional variance $Var(e_i / \vec{v}, \sigma_i^{0^*})$ by using two specific neural networks (denoted NN-VAR-H and NN-VAR-V) which have similar architectures to these of the NN-GMFs. All the computations were done in linear space. The inputs of the NN-VARs are v, $sin\ \chi$, $cos\ \chi$, $sin\ \theta$ and s_{i^a}, where v is the wind speed and s_{i^a} the output of the dedicated NN-GMF which approximates σ^o_j* (the NN-GMFs). Both NN-VARs are fully connected MLPs with two hidden layers of 8 and 6 neurons. They have a single output with an exponential function giving $Var(e_i / \vec{v}, \sigma_i^{0^*})$. The above computed variances are the sum of the variance var_1 due to instrumental noise, the variance var_2 due to the model and the variance var_3 due to geophysical phenomena (sea state, rain, and temperature).

NN-VAR-V and NN-VAR-H have been calibrated by using the calibration sets of the NN-GMFs. But we now use the log likelihood cost function introduced in Section 3 (equation 2). We minimize (2) with respect to the weights of NN-VAR-H and NN-VAR-V, where the control variables (the weights W_{ij} of the MLPs) only affect the $Var(e_i / \vec{v}, \sigma_i^{0^*})$.

Using a similar methodology as described in Section 5, we perform a χ^2-test on $Var(e_i / \vec{v}, \sigma_i^{0^*})$ to check the accuracy and the consistency of the values obtained for $Var(e_i / \vec{v}, \sigma_i^{0^*})$. **Figure 15** displays the results for an incidence angle of 36.1°. It is seen that the neural network methodology provides an estimate of the variance. When the test is rejected we computed the ratio (rt) of the empirical versus the NN-VAR standard deviation which was always such that $0.5 < rt < 2$.

In **Figure 16** we plot (a) NN-VAR-V against NN-GMF-V and (b) NN-VAR-H against NN-GMF-H at an incidence angle of 49°. We denote that the trend of the graphs of the NN-VAR relationship are quadratic and of the form of equation (3). The coefficients α, β and γ are dependent of the incidence angle. They are presented in table 3 at three different incidence angles; they are in quite good agreement with those provided by previous authors (Pierson, 1997). As var_1 of the order of 4% (Stoffelen and Anderson, 1997a) and var_2 which can be estimated using the techniques presented in Mejia *et al* (1998) is less than 10%, the variance var_3 is the most important one. Besides it is noticed that the wavy pattern of the curves is a function of the wind azimuth and wind speed.

Figure 17 displays the signal to noise ratio (so called K_p) at three different incidence angles with respect to the azimuth angle and at different wind speeds. The presented K_p are mainly due to geophysical noise as discussed above. Clearly this ratio is a function of the azimuth angle and the wind speed. The K_p values are quite high at low wind speed and decrease at high wind speed. At constant wind speed, the highest K_p are at cross-wind showing that the cross wind values are the most difficult to compute.

Figure 18 presents NN-GMF-V values for different wind speeds (white and black curves)

with respect to the azimuth angle for two distinct wind speed ranges and at an incidence angle of 36.1° against the NSCAT data set. In the same figure we plot bars corresponding to one and two standard deviations for some wind speeds and azimuth angles, the standard deviation being computed from NN-VAR results. It can be seen that the two NN-GMFs fit the data well and that they provide the conditional mean of the measurement as predict by NN theory [Thiria et al., 1993]. Moreover the estimation of the variance is quite realistic.

From the above results it is concluded that the NN-VARs give quite good estimates of the variance of NN-GMFs. The variance depends on the incidence angle, the wind azimuth and the wind speed. Previous estimations of the variance as those of the form described in Section 3 (equation 3) seem a rough approximation of the reality. A more detail analysis of the NSCAT variances will be given in a subsequent paper.

CONCLUSION

As shown in the statistical tests described above, the NSCAT GMFs estimated by using neural networks can be considered as good models of the NSCAT GMFs. Their biases are close to zero and their RMS are small except at low wind speeds. Due to the large temporal and geographical ranges of the data set used for the calibration, they can be considered as mean values corresponding to an average sea state and a mean sea surface temperature of 12°C.

In order to limit the strong non-linearity of the signal and owing to the large dynamical range of the sigma-0 values which is of several orders of magnitude, we decided to code them in dB as argued by Stoffelen and Anderson [1997a, b]. In the dB space the noise is not any more Gaussian (Stoffelen and Anderson, 1997a, b, Rufenach, 1998). This coding strongly limits the choice of potential cost functions used in the minimization phase since the log likelihood function (2) does not satisfy the statistical criteria in the dB space for estimating the a-posteriori probability P of the mean of the sigma-0 set constrained by the model (W and the

noise variance $Var(e_i)$). We thus chose a quadratic cost function of the form (5) which gives a correct estimation of the mean when dealing with neural networks (Bishop, 1995). In fact we have to face a dilemma: either to deal with a MLE estimation in the linear space or to work in the dB space for reducing the complexity of the problem and minimize a simple quadratic cost function. We choose the second solution from a practical point of view (the data are given in dB) and because we do not have a satisfactory representation of the variance of the noise.

The determination of the NN-GMFs is statistical and no *a-priori* hypotheses were done on their behavior. The biharmonic dependence with respect to the azimuth and the upwind-downwind modulation are retrieved by the two NN-GMFs. The up-wind and down wind maxima are at 0° and 180°. The two minima may differ from 90° and 270° and may not be of the same value. This slight difference is due to the fact that we do not impose the location of these minima *a-priori* and is embedded in the error bars of the function, as shown in Section 6. A sensitivity study on the error model similar to this done with ERS1 scatterometer data (Mejia *et al,* 1998) also shows some dispersion in the cross wind values. Thus we think that the slight variation in cross wind values is more related to statistical estimation rather than a geophysical phenomenon.

As the dynamical range of the NN-GMF-H is larger than this of NN-GMF-V, the use of two polarizations brings useful information which should improve the wind retrieval as already shown by the very good quality of the NSCAT winds retrieved by JPL NSCAT team. Since these NN-GMFs are good estimators of NSCAT-GMFs and differentiable functions of the variables (ν, χ and θ,) they might be used with efficiency in the wind retrieval algorithms which are based on the inversion of the GMFs.

Due to the flexibility of neural networks we were able to compute the variance of the two GMFs. In particular this leads us to compute the signal to noise ratio (so called K_p) which is a function of the incidence angle, the azimuth angle and the wind speed. The K_p values are

quite high at low wind speed and decrease at high wind speed. At a constant wind speed, the highest K_p are at cross-wind showing that the cross wind values are the most difficult to compute in agreement with the fact that the cross wind minimum are not exactly at 90° and 270°. Previous estimations of the variance as those of the form described in section 3 (equation 3) seem a rough approximation of the reality. This endorse our choice of not using the log likelihood equation as a cost function.

Comparison of the present NN-GMFs with respect to data and to other GMFs are presented in a companion paper (Bentamy *et al*, this issue). Effects of secondary phenomena such as the long wave height and direction, and the sea surface temperature have been neglected. Investigation of the effect of these parameters on GMF will be performed in a subsequent work.

The two NN-GMFs and the two NN-VARs can be expressed as Fortran subroutines and disseminated to potential users.

Acknowledgments

We would like to thank the CERSAT/IFREMER who provided the collocations between NSCAT sigma-0 and the analyzed wind vectors of the ECMWF Model. Dr D. Cornford did pertinent comments on a previous version of the paper. The present study was supported by the EC program NEUROSAT (ENV4-CT96-0314).

ANNEX 1

The bias is defined as:

$$\overline{\text{BIAS}} = \frac{\sum \left(\sigma_{\text{NN-GMF}} - \sigma_{\text{ERS-1}}\right)}{\text{N}}$$

and the RMS:

$$\text{RMS} = \sqrt{\frac{\sum \left(\sigma_{\text{NN-GMF}} - \sigma_{\text{ERS-1}}\right)^2}{\text{N}}}$$

where: $\sigma_{\text{NN-GMF}}$ is the sigma-0 computed by the GMF,

σ_{ERS-1} is the sigma-0 observed by NSCAT,

N is the number of collocated pairs.

BIBLIOGRAPHY

ANDERSSON E., J. HASELER, P. UNDEN, P. COURTIER, G. KELLY, D. VASILJEVIC, C. BRANKOVIC, C. CARDINALI, C. GAFFARD, A. HOLLINGSWORTH, C. JAKOB, P. JANSSEN, E. KLINKER, A. LANZINGER, M. MILLER, F. RABIER, A. SIMMONS, B. STRAUSS, J.-N. THEPAUT AND P.VITERBO: THE ECMWF IMPLEMENTATION OF THREE-DIMENSIONAL VARIATIONAL ASSIMILATION (3D-VAR). III: EXPERIMENTAL RESULTS, Q. J. R, METEOROL. SOC., 124, PP. 1831-1860,1998.

BADRAN F., S. THIRIA, AND M. CREPON: WIND AMBIGUITY REMOVAL BY THE USE OF NEURAL NETWORK TECHNIQUES. *J. GEOPHYS. RES.,* 96, 20521-20529, 1991.

BENTAMY A., B. CHAPRON, P. QUEFFELOU, Y. KILFEN, C. KASTSAROS, S. POULIQUEN AND C. MEJIA: CHARACTERIZATION OF NSCAT MEASUREMENTS BASED ON ERS2 WIND VECTOR OBSERVATIONS. *J. GEOPHYS. RES* (THIS ISSUE).

BENTAMY A., Y. QUILFEN, P. QUEFFEULOU AND A. CAVANIE: CALIBRATION OF ERS-1 SCATTEROMETER C-BAND MODEL, IFREMER TECHNICAL REPORT, DRO/OS-94-01, IFREMER, 72 P, 1994.

Bishop C. M.: NEURAL NETWORKS FOR PATTERN RECOGNITION, OXFORD UNIVERSITY PRESS, 482 P., 1995.

BLIVEN L. F., J. P. GIOVANANGELI, R. H. WANNINKHOF AND B. Chapron : A LABORATORY STUDY OF FRICTION VELOCITY ESTIMATES FROM SCATTEROMETRY : LOW AND HIGH REGIMES. *INT. J. REMOTE SENSING* , 1775-1785, 1993.

CAVANIÉ A. and D. OFFILER : ERS1 Wind Scatterometer : Wind Extraction and Ambiguity Removal. *Proceedings of IGARS 86 Symposium, Zurich,* (ESA SP-254), 1986

Chen K.S., A.K. Fung AND D.E. Weissman : A BACKSCATTERING MODEL FOR THE OCEAN SURFACE, *IEEE, TRANS. ON GEOSCI. AND REM. SENS. ,* 30, 4, PP 811-817, 1992.

COURTIER P., E. ANDERSSON, W. HECKLEY, J. PAILLEUX, D. VASILJEVIC, M. HAMRUD, A. HOLLINGSWORTH, F. RABIER AND M. FISHER: THE ECMWF IMPLEMENTATION OF THREE-DIMENSIONAL VARIATIONAL ASSIMILATION (3D-VAR). I: FORMULATION, *Q. J. R. METEOROL. SOC*., 124, PP. 1783-1807, 1998.

Donelan M. A. : AIR-SEA INTERACTION , IN *THE SEA*, 9, OCEAN ENGINEERING SCIENCE, EDS B. LEMEHAUTE AND D. HANES, WILEY, NEW-YORK, 239-292, 1990.

Donelan M.A. AND W.J. Pierson : RADAR SCATTERING AND EQUILIBRIUM RANGES IN WIND-

GENERATED WAVES WITH APPLICATION TO SCATTEROMETRY, *J. GEOPHYS. RES.,* 92, 4971-5029, 1987.

Donelan M.A., F. Dobson, S. Smith AND R. Anderson : DEPENDANCE OF SEA SURFACE ROUGHNESS ON WAVE DEVELOPMENT, *J. GEOPHYS. RES.,* 98, 2143-2149, 1993.

FISCHER R. E.: STANDARD DEVIATION OF SCATTEROMETER MEASUREMENTS FROM SPACE, *IEEE TRANS. ON GEOSCIENCE ELECTRONICS,* VOL. GE-10, NO. 2, PP. 106-113, 1972.

Janssen P. AND P.M. Woiceshyn : WAVE AGE AND THE SCATTEROMETER RETIEVAL ALGORITHM IN ERS1 GEOPHYSICAL VALIDATION : WORKSHOP PROCEEDINGS, ESA-WPT-36, ED. E. ATTEMA, PP141-143, 1992.

KAHMA K.K. AND M.A. DONELAN : A LABORATORY STUDY OF THE MINIMUM WIND SPEED FOR WIND WAVE GENERATION : J. FLUID MECH., 192, 339-364, 1993.

KREYSZIG E. : ADVANCED ENGENEERING MATHEMATICS, 939P., *J. WILEY AND SONS, ED. NEW YORK, CHICHESTER, BRISBANE, TORONTO,* 1979

LIU Y. AND W. J. PIERSON : COMPARISONS OF SCATTEROMETER MODELS FOR THE AMI ON ERS-1: THE POSSIBILITY OF SYSTEMATIC AZIMUTH ANGLE BIASES OF WIND SPEED AND DIRECTION. *IEEE TRANS. ON GEOS. AND REMOTE SENSING*, 32, 626, 635. 1994.

LONG A. E.: TOWARDS A C-BAND RADAR SEA ECHO MODEL FOR THE ERS-1 SCATTEROMETER, IN *PROC. OF THE 3RD INTERNATIONAL COLLOQUIUM ON SPECTRAL SIGNATURE, EUR. SPACE AGENCY SPEC. PUBL.,* ESA SP-247, 29-34, 1985.

MEJIA C., S. THIRIA, F. BADRAN, AND M. CREPON: A NEURAL NETWORK APPROACH FOR WIND RETRIEVAL FROM THE ERS-1 SCATTEROMETER DATA. IN *IEEE OCEAN94 PROCEEDINGS*, 1, BREST-SEPT. 13-16, 1994.

MEJIA C., S. THIRIA, N. TRAN, M. CREPON, H. ROQUET, P. RICHAUME, F. BADRAN: The Neural Network GMFs NSCAT scatterometers. *Proc. NSCAT SWT meeting*, Hawaii, January 1997.

MEJIA C., S. THIRIA, F. BADRAN, N. TRAN and M. CREPON : Determination of the Geophysical Model Function of ERS1 Scatterometer by the use of Neural Networks. *J. Geophys. Res.*, 103, 12,853-12,868, 1998.

Nghiem S., F. LI, H. Lou AND G. Neuman : OCEAN REMOTE SENSING WITH AIRBORNE KU-BAND SCATTEROMETER, *OCEAN 93 PROCEEDINGS* , 1, 20-24, VICTORIA, BC, 1993**.**

PIERSON W. J.: PROBABILITIES AND STATISTIC FOR BACKSCATTER ESTIMATES OBTAINED BY A SCATTEROMETER , *J. GEOPHYS. RES., 94,* 9743-19759, 1989.

PIERSON W. J.: THE USE OF THE MODELING ERROR FOR THE RECOVERY OF NSCAT WINDS. *PROC. NSCAT SWT MEETING*, HAWAII, JANUARY 1997..

Plant W.J.: A TWO SCALE MODEL OF SHORT WIND GENERATED WAVES AND SCATTEROMETRY, *J. GEOPHYS. RES., 91,* 10735-10749, 1986.

RICHARD M. D. AND R. P. LIPPMANN: NEURAL NETWORK CLASSIFIERS ESTIMATE BAYESIAN A-POSTERIORI PROBABILITIES. *NEURAL COMPUTATION* 3 (4), 461-483, 1991.

RUFENACH C. : Comparison of Four ERS-1 Scatterometer Wind retrieval Algorithms with buoys measurements. *J. Atm. Ocean Tech..,* 304-313, 1998.

STOFFELEN A. : Toward the true near-surface wind speed error: Error modelling and calibration using triple correlation . *J. Geophys. Res., 103,* 7755-7776, 1998.

STOFFELEN A. and D. ANDERSON : Scatterometer data interpretation : Measurement Space and Inversion. *J. Atm. Ocean Tech..,* 1298-1313, 1997a.

STOFFELEN A. AND D. ANDERSON: SCATTEROMETER DATA INTERPRETATION : ESTIMATION AND VALIDATION OF THE TRANSFER FUNCTION CMOD4. *J. GEOPHYS. RES.* 102, 5767-5780, 1997B.

THIRIA S., F. BADRAN, C. MEJIA AND M. CREPON: A NEURAL NETWORK APPROACH FOR MODELLING NON LINEAR TRANSFER FUNCTIONS : APPLICATION FOR WIND RETRIEVAL FROM SPACEBORNE SCATTEROMETER DATA. *J. GEOPHYS. RES.* 98, 22827-22841, 1993.

Weissman D. E., K. L.Davidson, R. Brown, C. A. Friehe AND F. Li: THE RELATIONSHIP BETWEEN MICROWAVE RADAR CROSS SECTION AND BOTH WIND SPEED AND WIND STRESS: MODEL FUNCTION STUDIES USING FRONTAL AIR-SEA INTERACTION EXPERIMENT DATA, *J. GEOPHYS. RES.* 99, 22827-22841, 1994.

WOICESHYN P. M, M. G. WURTELE, D. H. BOGGS, L. F. MCGLODRICK, AND S. PETEHERYCH : THE NECESSITY FOR A NEW PARAMETERIZATION OF AN EMPIRICAL MODEL FOR WIND/OCEAN SCATTEROMETRY. *J. GEOPHYS. RES.* 91, 2273-2288, 1986.

TABLES

WVC 11 VERTICAL POLARIZATION - mean incidence angle of 22.6º -				
Speed Interval min (m/s)	max (m/s)	N	bias (dB)	RMS (dB)
2	4	21748	0.154	4.857
4	6	37874	0.271	1.999
6	8	40078	0.029	1.006
8	10	24745	-0.032	0.857
10	12	9172	-0.019	0.827
12	14	2594	0.112	0.806
14	16	1179	0.122	0.857
16	18	359	0.116	0.669
18	20	91	0.233	0.426
20	22	0	-----	-----
22	24	36	-0.133	0.639

WVC 07 VERTICAL POLARIZATION - mean incidence angle of 36.9º -				
Speed Interval min (m/s)	max (m/s)	N	bias (dB)	RMS (dB)
2	4	7131	0.043	5.117
4	6	11501	0.012	3.246
6	8	12691	0.098	2.017
8	10	8610	-0.003	1.562
10	12	2711	-0.210	1.377
12	14	951	-0.082	1.352
14	16	246	0.436	1.416
16	18	87	0.510	0.794
18	20	60	0.254	0.875
20	22	16	0.385	0.647
22	24	32	0.281	0.392

WVC 02 VERTICAL POLARIZATION - mean incidence angle of 49.7º -				
Speed Interval min (m/s)	max (m/s)	N	bias (dB)	RMS (dB)
2	4	20502	-0.016	5.639
4	6	33026	0.479	3.659
6	8	36815	0.558	2.511
8	10	23776	0.425	1.806
10	12	7985	0.095	1.580
12	14	2845	0.228	1.147
14	16	839	0.336	1.086
16	18	345	0.771	1.283
18	20	173	0.712	0.946
20	22	79	0.460	0.645
22	24	48	0.381	0.599

Table 1a : Bias and RMS of NN-GMF-V at three different incidence angles with respect to the wind speed. N represents the number of data used in each wind speed interval for calibrating NN-GMF-V.

WVC 11 HORIZONTAL POLARIZATION
- mean incidence angle of 22.6º -

Speed Interval min (m/s)	max (m/s)	N	bias (dB)	RMS (dB)
2	4	15085	-0.097	5.074
4	6	25412	0.234	2.223
6	8	26094	0.160	1.164
8	10	18555	0.125	0.933
10	12	6152	-0.007	0.836
12	14	2092	0.060	0.777
14	16	812	0.029	0.870
16	18	290	0.077	0.647
18	20	81	0.147	0.418
20	22	18	0.306	0.512
22	24	12	-0.134	0.297

WVC 07 HORIZONTAL POLARIZATION
- mean incidence angle of 36.8º -

Speed Interval min (m/s)	max (m/s)	N	bias (dB)	RMS (dB)
2	4	15128	-0.498	5.613
4	6	24145	-0.054	3.392
6	8	26220	0.226	2.047
8	10	19186	0.194	1.622
10	12	6046	0.032	1.531
12	14	2355	-0.016	1.360
14	16	729	0.096	1.351
16	18	162	0.523	0.941
18	20	113	0.311	0.737
20	22	20	0.112	0.610
22	24	32	-0.119	0.392

WVC 02 HORIZONTAL POLARIZATION
- mean incidence angle of 50.1º -

Speed Interval min (m/s)	max (m/s)	N	bias (dB)	RMS (dB)
2	4	15270	0.049	5.568
4	6	23745	0.023	4.359
6	8	27630	0.215	2.821
8	10	18462	0.100	2.150
10	12	6607	-0.073	2.293
12	14	2322	-0.016	2.193
14	16	973	-0.066	1.641
16	18	397	0.689	1.573
18	20	81	0.538	1.509
20	22	0	------	-----
22	24	0	------	-----

Table 1b : Bias and RMS of NN-GMF-H at three different incidence angles with respect to the wind speed. N represents the number of data used in each wind speed interval for calibrating NN-GMF-H.

A1 VERTICAL POLARIZATION							
vitesse	Inc.20°	Inc.25°	Inc.30°	Inc.35°	Inc.40°	Inc.45°	Inc.50°
4	-0.0040	0.0729	0.1618	0.2187	0.2363	0.2271	0.2041
6	0.0057	0.0970	0.1858	0.2426	0.2650	0.2632	0.2475
8	-0.0168	0.0632	0.1327	0.1776	0.1983	0.2008	0.1914
10	-0.0337	0.0284	0.0774	0.1108	0.1297	0.1360	0.1325
12	-0.0427	0.0025	0.0351	0.0599	0.0784	0.0891	0.0919
14	-0.0464	-0.0152	0.0052	0.0242	0.0433	0.0590	0.0687
16	-0.0471	-0.0267	-0.0150	-0.0001	0.0202	0.0410	0.0578
18	-0.0461	-0.0338	-0.0280	-0.0159	0.0054	0.0308	0.0544
20	-0.0440	-0.0380	-0.0359	-0.0257	-0.0037	0.0252	0.0547
22	-0.0411	-0.0400	-0.0400	-0.0309	-0.0089	0.0222	0.0561
24	-0.0374	-0.0401	-0.0412	-0.0327	-0.0112	0.0206	0.0569

A2 VERTICAL POLARIZATION							
Vitesse (m/s)	Inc.20°	Inc.25°	Inc.30°	Inc.35°	Inc.40°	Inc.45°	Inc.50°
4	0.1320	0.1746	0.2529	0.3181	0.3570	0.3769	0.3865
6	0.1655	0.2309	0.3180	0.3835	0.4215	0.4411	0.4504
8	0.1910	0.2612	0.3393	0.3951	0.4276	0.4451	0.4538
10	0.2204	0.2831	0.3452	0.3885	0.4147	0.4296	0.4377
12	0.2511	0.3007	0.3452	0.3763	0.3963	0.4088	0.4164
14	0.2793	0.3147	0.3429	0.3627	0.3769	0.3873	0.3945
16	0.3025	0.3252	0.3394	0.3490	0.3576	0.3659	0.3729
18	0.3192	0.3316	0.3346	0.3352	0.3384	0.3443	0.3509
20	0.3288	0.3333	0.3278	0.3210	0.3190	0.3221	0.3280
22	0.3310	0.3297	0.3184	0.3058	0.2989	0.2990	0.3035
24	0.3263	0.3208	0.3059	0.2894	0.2784	0.2751	0.2777

Table 2a . A1 and A2 coefficients of the Fourier series expansion of the NN-GMF-V as a function of the wind speed at different incidence angles.

A1 HORIZONTAL POLARIZATION							
vitesse	Inc.20°	Inc.25°	Inc.30°	Inc.35°	Inc.40°	Inc.45°	Inc.50°
4	0.0054	0.0799	0.1609	0.2385	0.3048	0.3577	0.4002
6	-0.0030	0.0841	0.1791	0.2731	0.3573	0.4259	0.4775
8	0.0117	0.1040	0.1982	0.2864	0.3627	0.4245	0.4720
10	0.0152	0.1082	0.1994	0.2804	0.3462	0.3962	0.4323
12	0.0046	0.0938	0.1802	0.2552	0.3141	0.3563	0.3842
14	-0.0131	0.0694	0.1496	0.2193	0.2737	0.3119	0.3360
16	-0.0327	0.0427	0.1166	0.1816	0.2328	0.2691	0.2919
18	-0.0506	0.0185	0.0871	0.1484	0.1975	0.2329	0.2555
20	-0.0645	0.0001	0.0650	0.1238	0.1718	0.2070	0.2300
22	-0.0730	-0.0110	0.0520	0.1097	0.1574	0.1928	0.2164
24	-0.0756	-0.0145	0.0482	0.1061	0.1542	0.1904	0.2147

A2 HORIZONTAL POLARIZATION							
vitesse	Inc.20°	Inc.25°	Inc.30°	Inc.35°	Inc.40°	Inc.45°	Inc.50°
4	0.0461	0.1271	0.1838	0.2157	0.2279	0.2271	0.2199
6	0.1448	0.2156	0.2650	0.2930	0.3044	0.3053	0.3008
8	0.2276	0.2920	0.3370	0.3607	0.3669	0.3619	0.3511
10	0.2763	0.3357	0.3782	0.4010	0.4061	0.3987	0.3841
12	0.2967	0.3512	0.3917	0.4145	0.4206	0.4138	0.3990
14	0.2993	0.3495	0.3878	0.4107	0.4182	0.4132	0.3998
16	0.2922	0.3387	0.3751	0.3977	0.4065	0.4034	0.3921
18	0.2803	0.3238	0.3586	0.3811	0.3908	0.3895	0.3801
20	0.2664	0.3077	0.3412	0.3637	0.3743	0.3746	0.3671
22	0.2523	0.2918	0.3245	0.3471	0.3588	0.3605	0.3546
24	0.2386	0.2769	0.3092	0.3322	0.3448	0.3479	0.3437

Table.2b . A1 and A2 coefficients of the Fourier series expansion of the NN-GMF-H as a function of the wind speed at different incidence angles.

Fit of the Variance by a second order Polynome

WVC	Mean Incidence angle	α	β	γ
11	22.19°	3.863e-03	1.944e-04	1.449e-02
07	36.31°	2.536e-02	3.918e-03	1.200e-04
02	49.63°	2.523e-02	2.075e-03	1.241e-05

Table 3 : Coefficients α, β, γ, given by a least square fit of the variance NN-VAR-V by a second order Polynome corresponding to equation 3

FIGURES

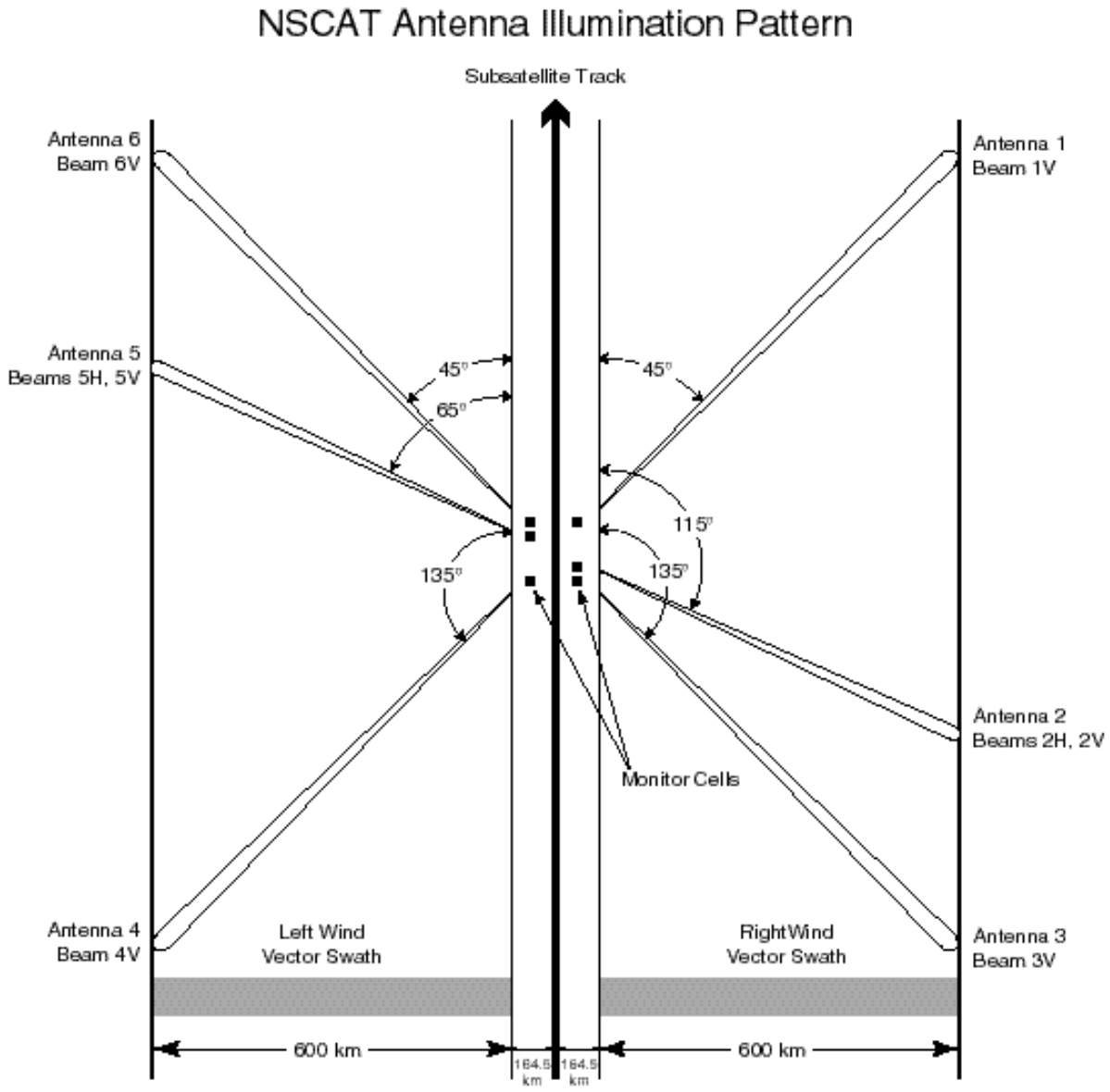

Fig. 1 : NSCAT antenna illumination pattern and the two swaths.

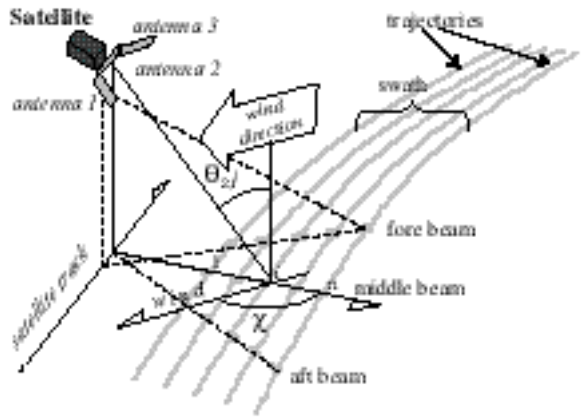

Fig. 2 : Definition of geophysical parameters: θ the incidence, χ the azimuth angle.

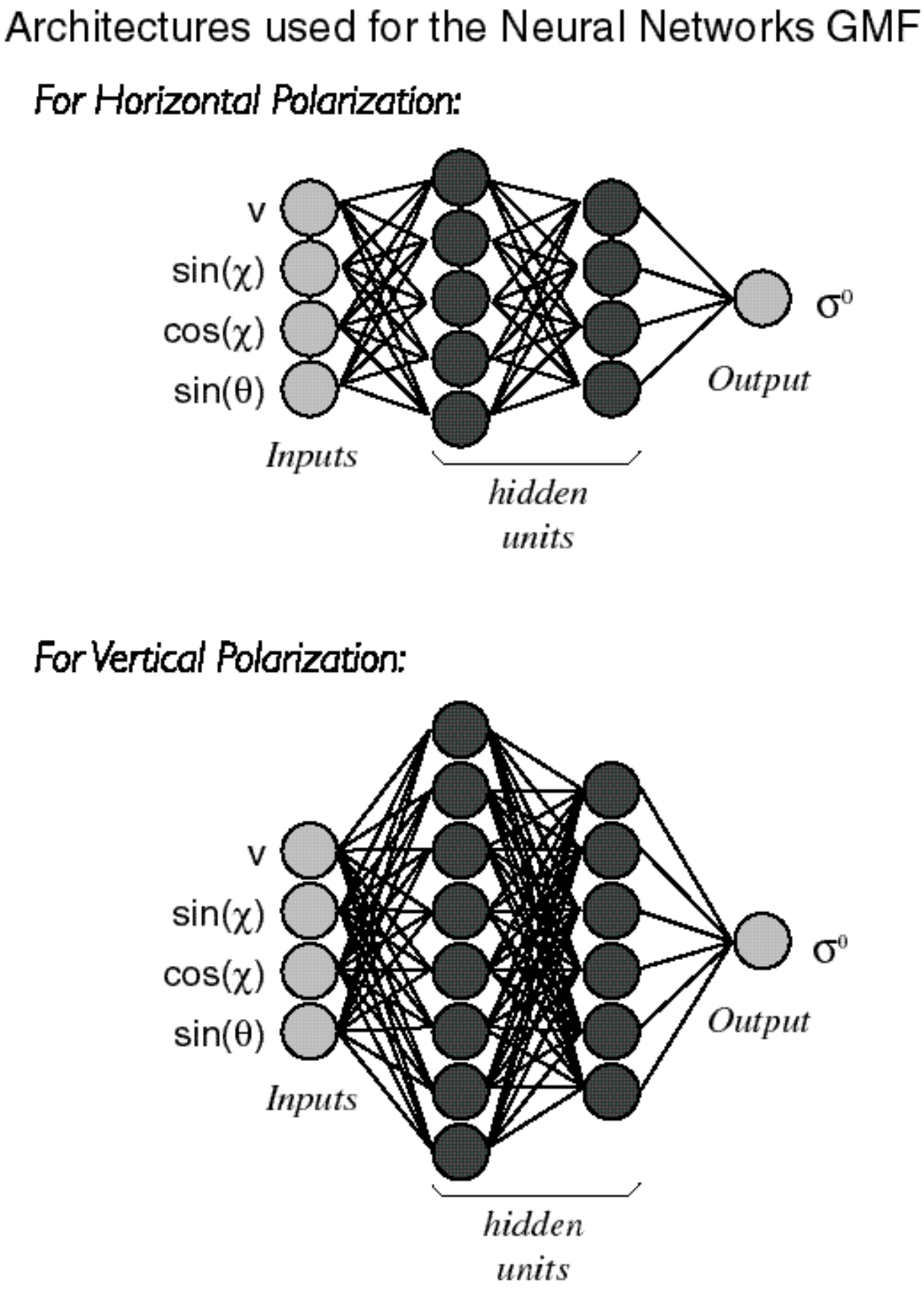

Fig. 3 : Architecture of the neural networks : (a) NN-GMF-H, (b) NN-GMF-V.

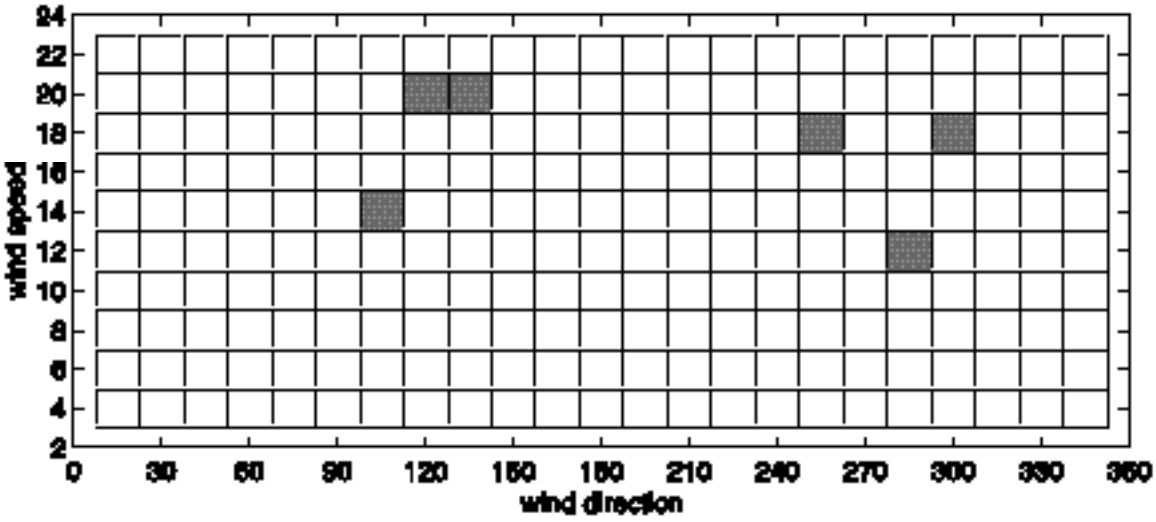

Fig. 4 : Student Test for the NN-GMF-V at an incidence angle of 36° with respect to the wind azimuth and for different wind speeds. When the pixels are white, the test is satisfied with a confidence level of 95% (at a significance level of 5%).

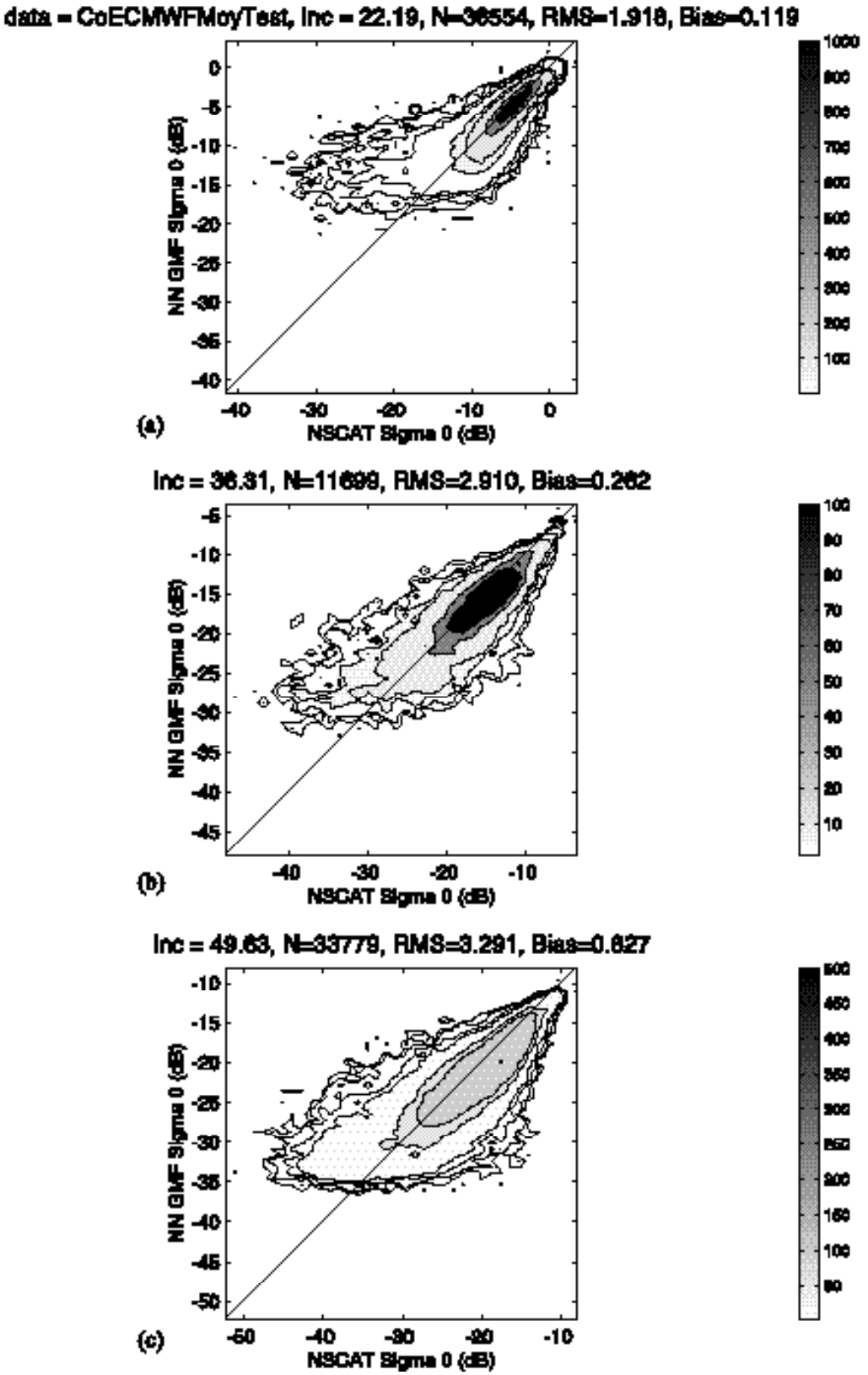

Fig. 5 : Scatter plots of NN-GMF-V versus the NSCAT sigma-0 at three incidence angles : (a) θ=22°; (b) θ=36°; (c) θ=49°5. The darker the area, the denser the data number. The scale is given in thousands of points.

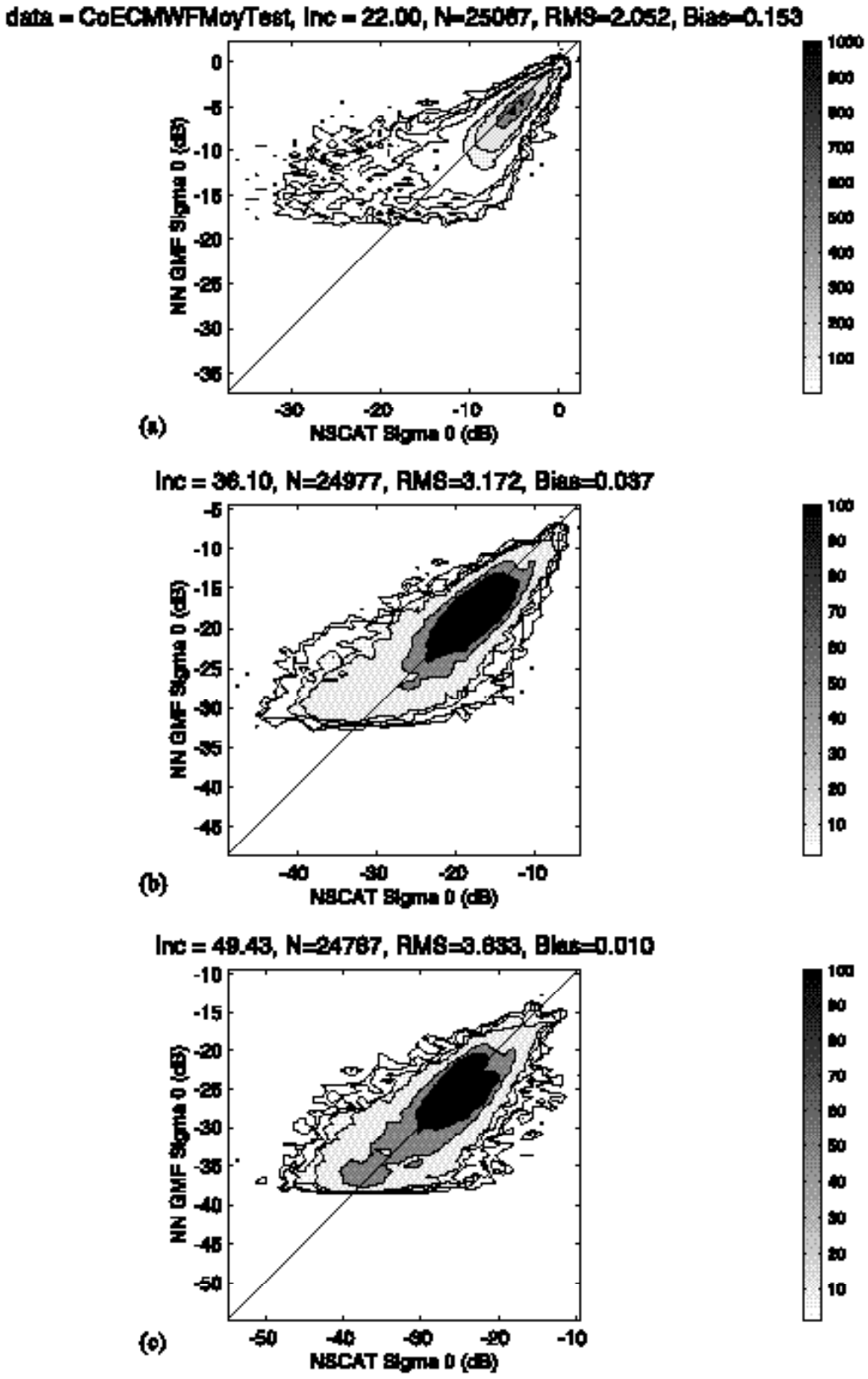

Fig. 6 : Scatter plots of NN-GMF-H versus the NSCAT sigma-0 at three incidence angles. (a) θ=22°; (b) θ=36°; (c) θ=49°5. The darker the area, the denser the data number. The scale is given in thousands of points.

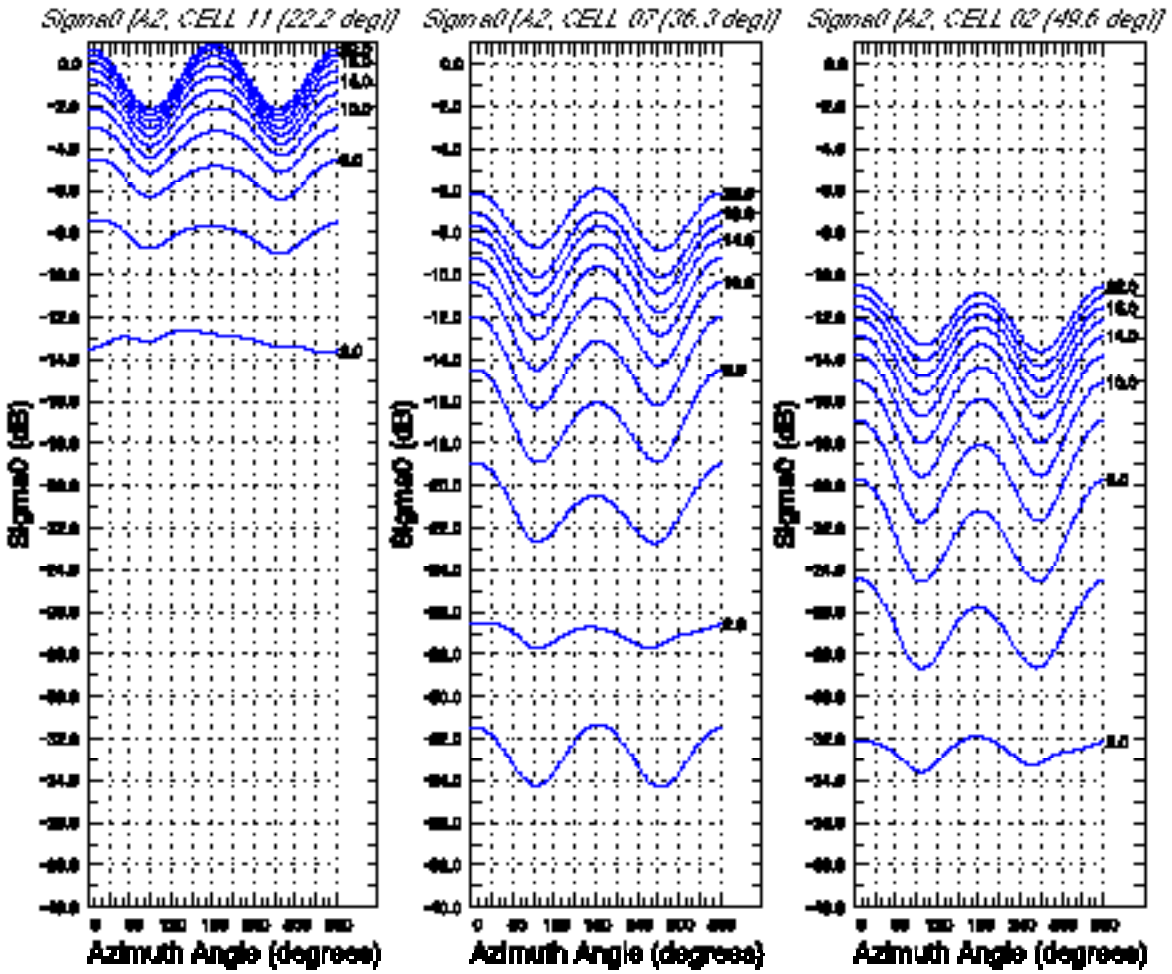

Fig. 7 : Sigma-0 (in dB.) of the NN-GMF-H function with respect to the azimuth angle at different wind speeds at three incidence angles. (a) θ=22°; (b) θ=36°; (c) θ=49°5.

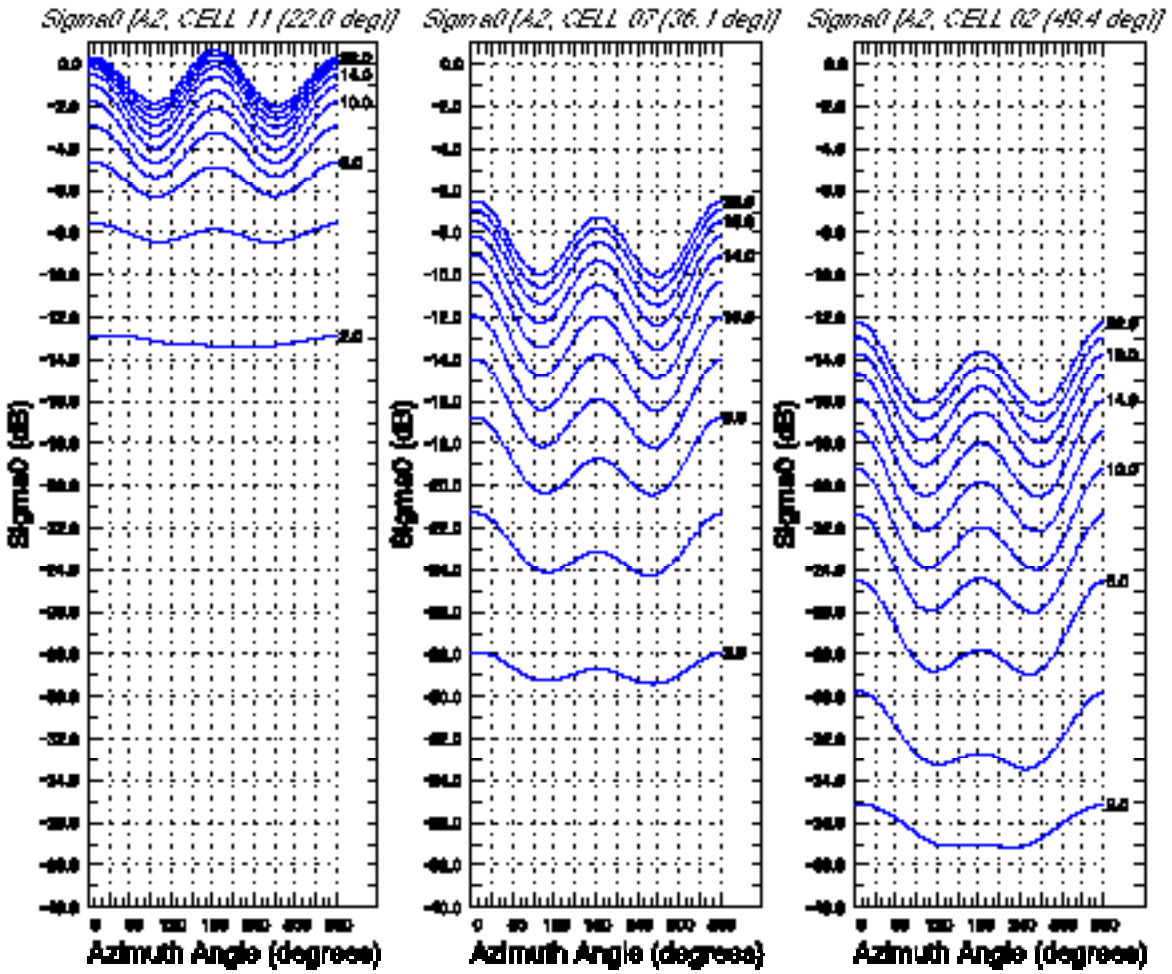

Fig. 8 : Sigma-0 (in dB.) of the NN-GMF-V function with respect to the azimuth angle at different wind speeds at three incidence angles. (a) θ=22°; (b) θ=36°; (c) θ=49°5..

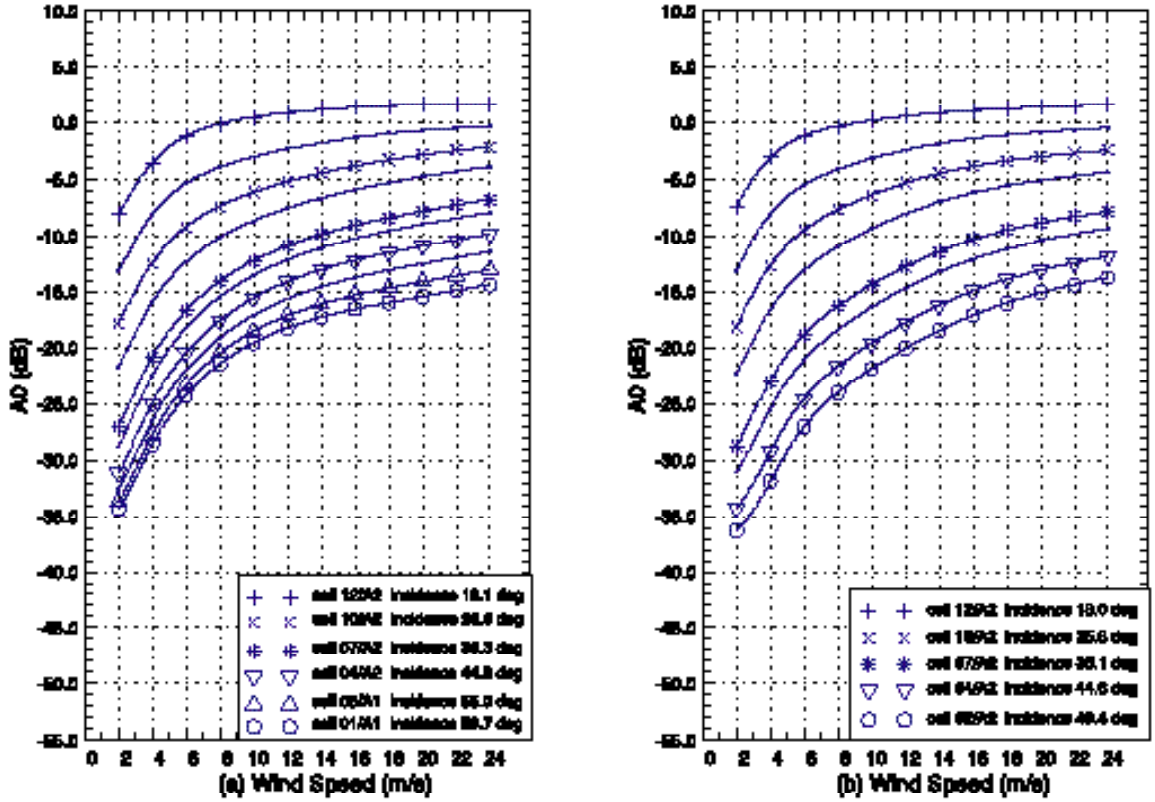

Fig. 9 : Mean values (A_0 Fourier coefficient) of (a) NN-GMF-V and (b) NN-GMF-H versus the wind velocity at different incidence angles. These values are given in dB.

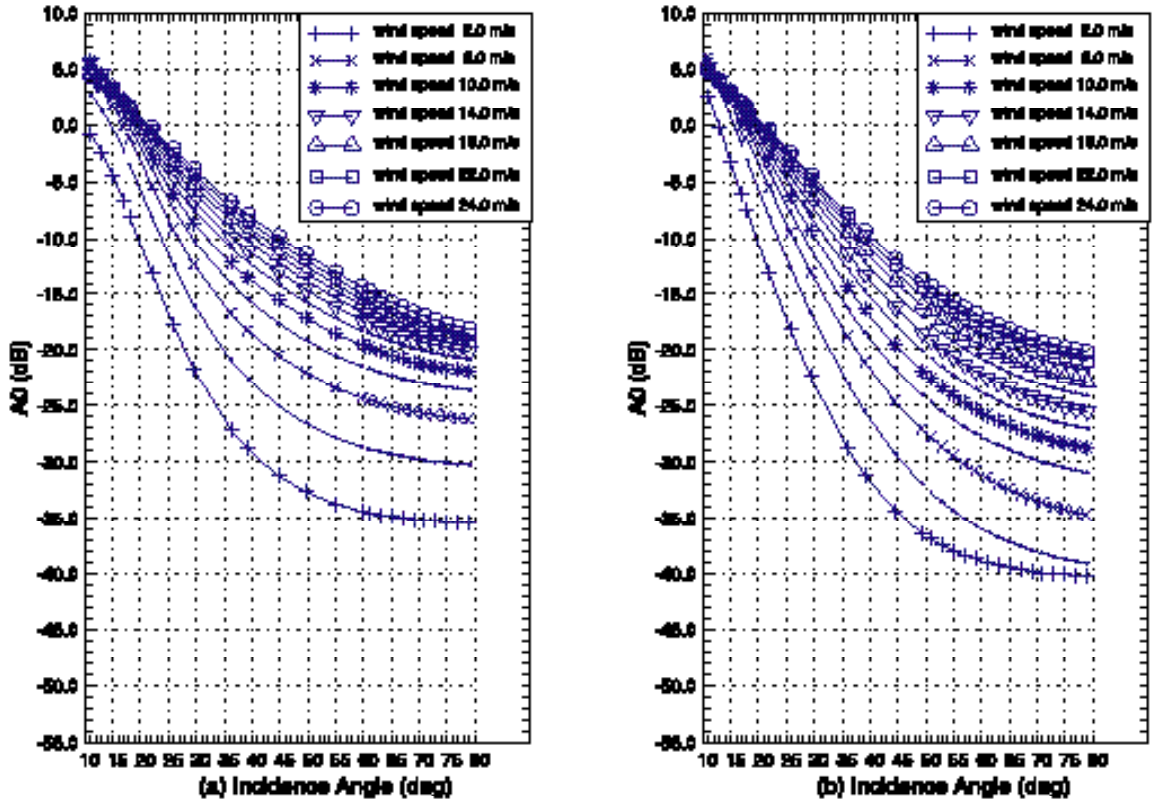

Fig. 10 : Mean values (A_0 Fourier coefficient) of (a) NN-GMF-V and (b) NN-GMF-H versus the incidence angle at different wind velocity. These values are given in dB.

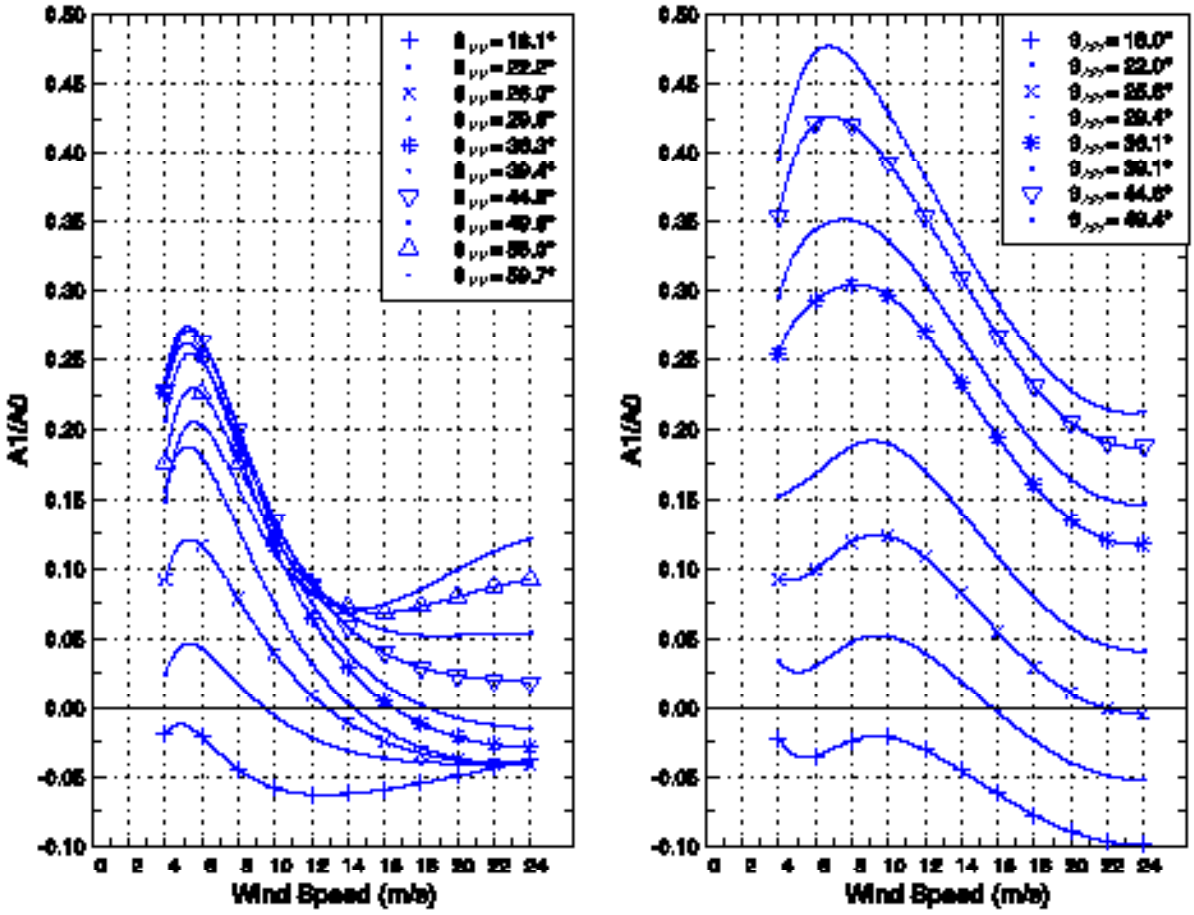

Fig. 11 : Up-wind minus down-wind values (A_1 Fourier coefficient) of (a) NN-GMF-V and (b) NN-GMF-H versus wind velocity at different incidence angles. All these values are given in linear scale.

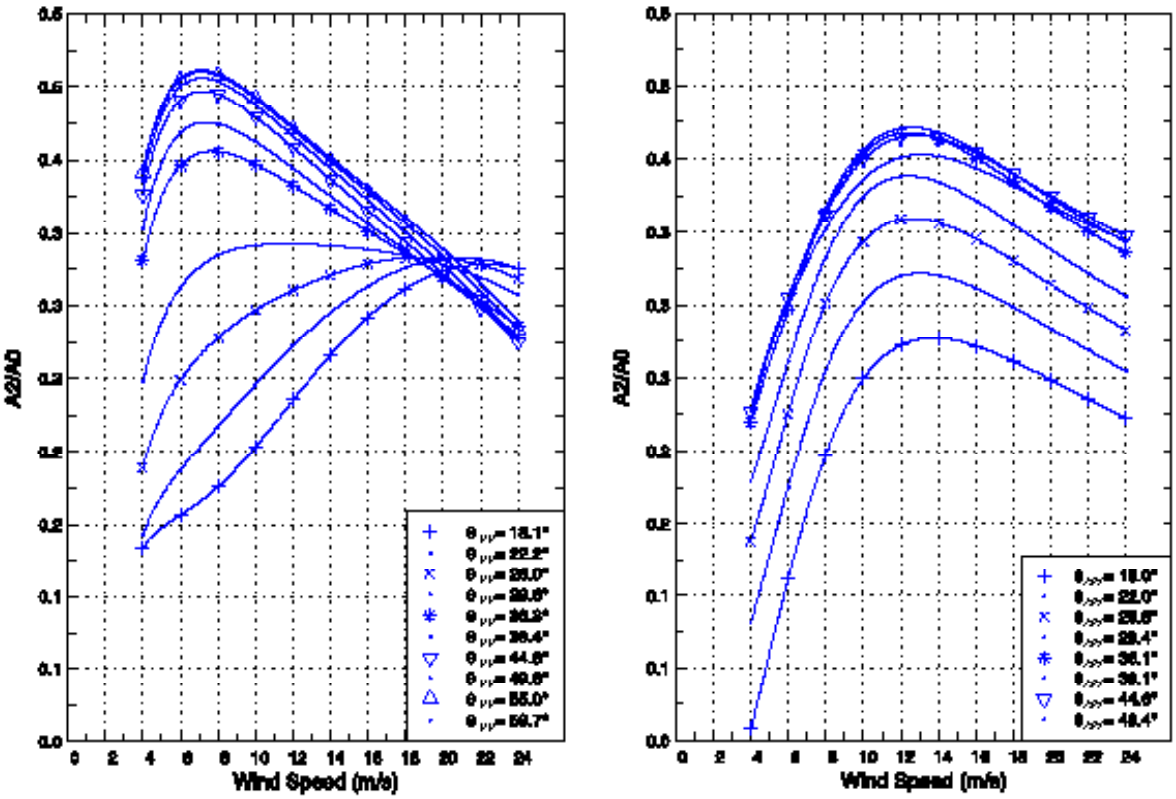

Fig. 12 : Up-wind minus cross wind values (A_2 Fourier coefficient) of (a) NN-GMF-V and (b) NN-GMF-H versus wind velocity at different incidence angles. All these values are given in linear scale.

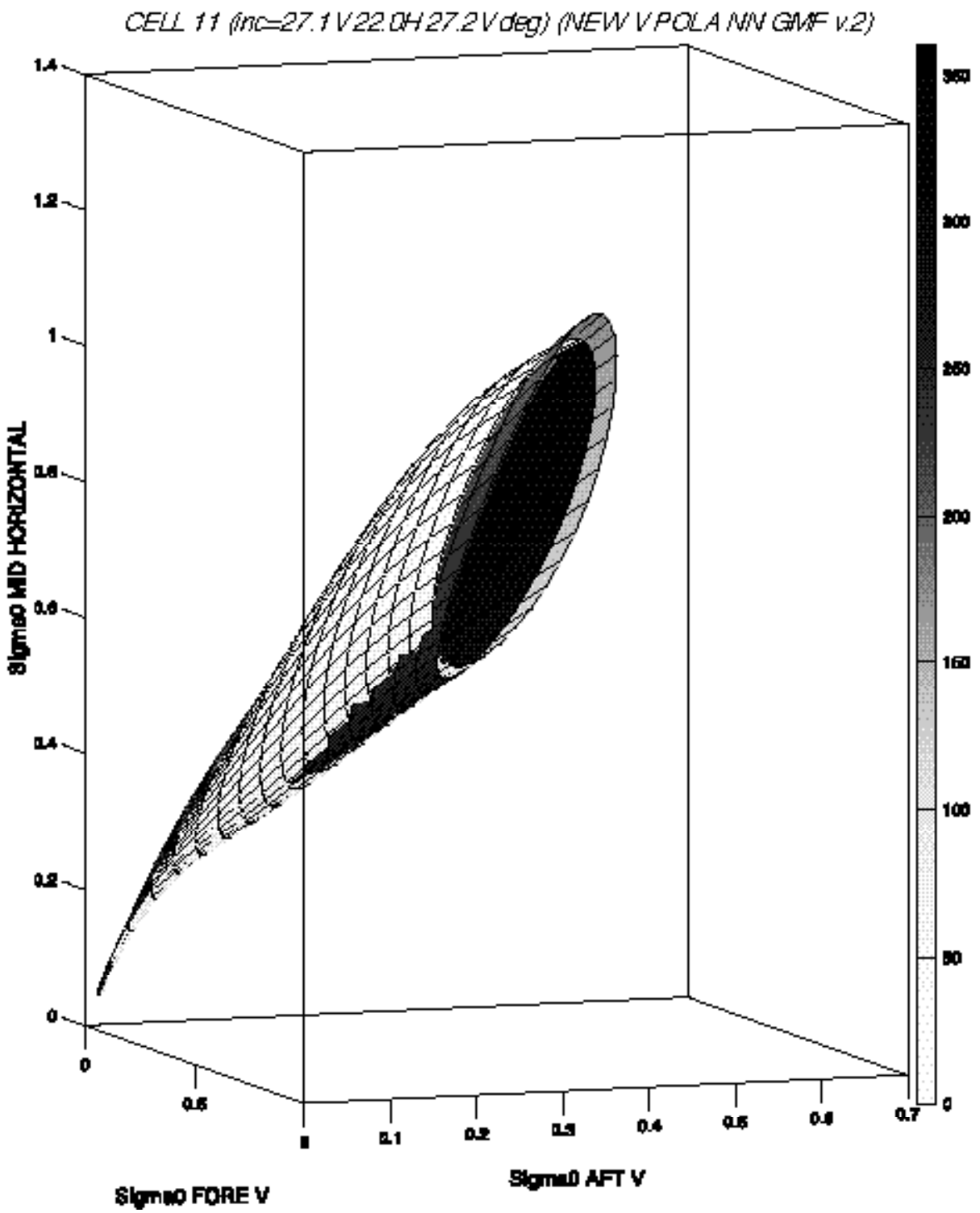

Fig. 13 **:** Three-dimensional view of a NN-GMF surface corresponding to wind vector solution in the sigma-0 space (σ^1, σ^2, σ^3), where σ^1 and σ^3 correspond to the vertical polarization at an incidence angle of 27° (fore and aft beams respectively) and σ^2 to the horizontal polarization at an incidence angle of 22° (mid beam).

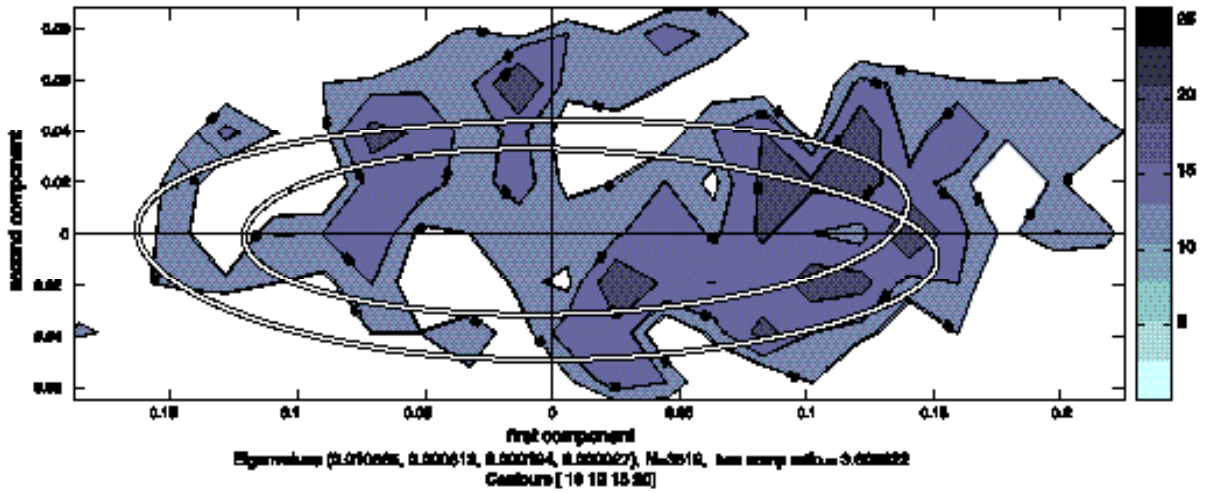

Fig 14 : Simplified projection of the NSCAT cone in the V.V.H. V space against the data corresponding to a wind speed of 8 ms^{-1} and incidence angles of 27°, 22°, 22° and 27°. The darker the shade, the denser the measurements. The scale is given in thousands of points.

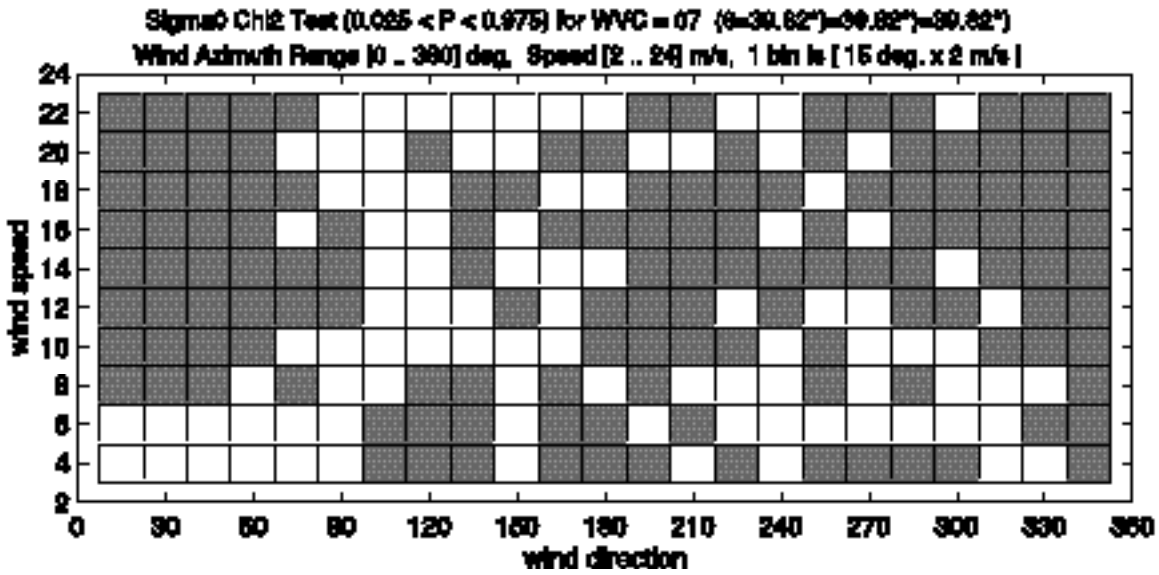

Fig. 15: Chi-2 Test for the NN-GMF-V at an incidence angle of 36° with respect to the wind azimuth and for different wind speeds. When the pixels are white, the test is satisfied with a confidence level of 95% (at a significance level of 5%).

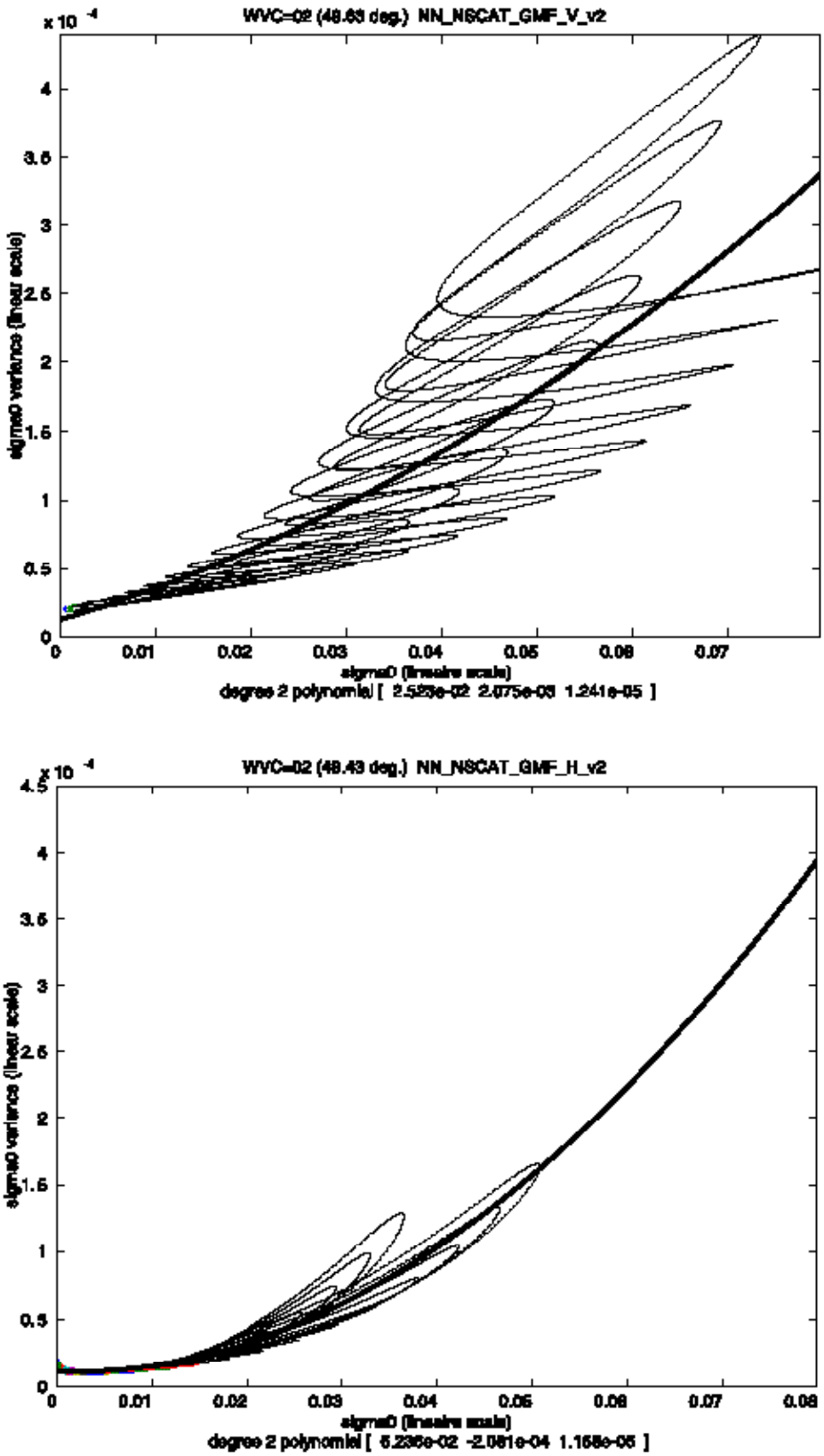

Fig. 16: (a) NN-VAR-V against NN-GMF-V, (b) NN-VAR-H against NN-GMF-H with respect to the wind speed at an incidence of 49°. The trend of the graph (heavy black line) of the NN-VAR relationship is quadratic and of the form of equation (3). The curly pattern of the curve (light line) is a function of the wind azimuth for different speed.

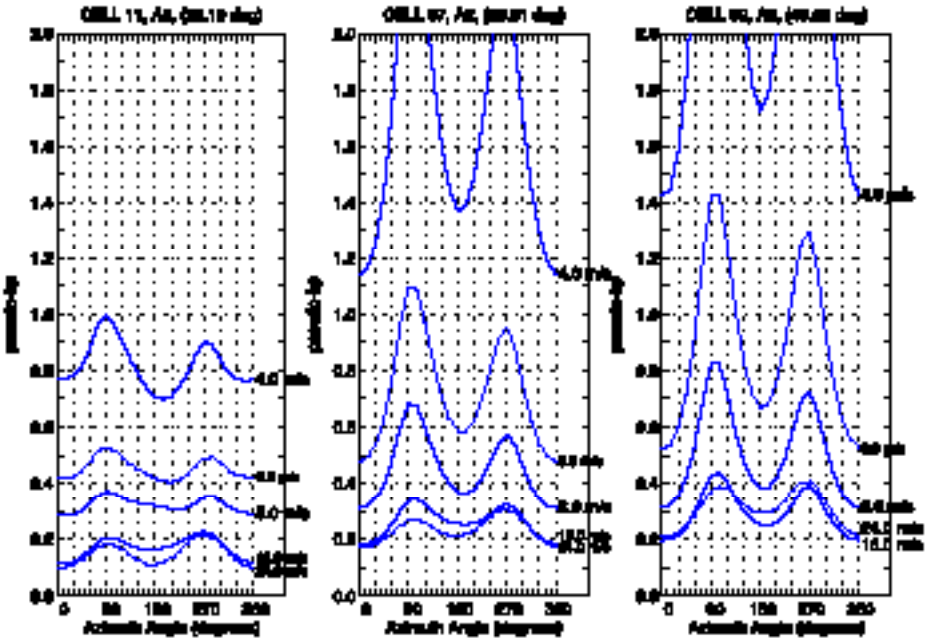

Fig 17 : Signal to noise ratio (so called Kp) corresponding to NN-GMF-V at three different incidence angles (22°, 36°, 49°) with respect to the azimuth angle and at different wind speeds.

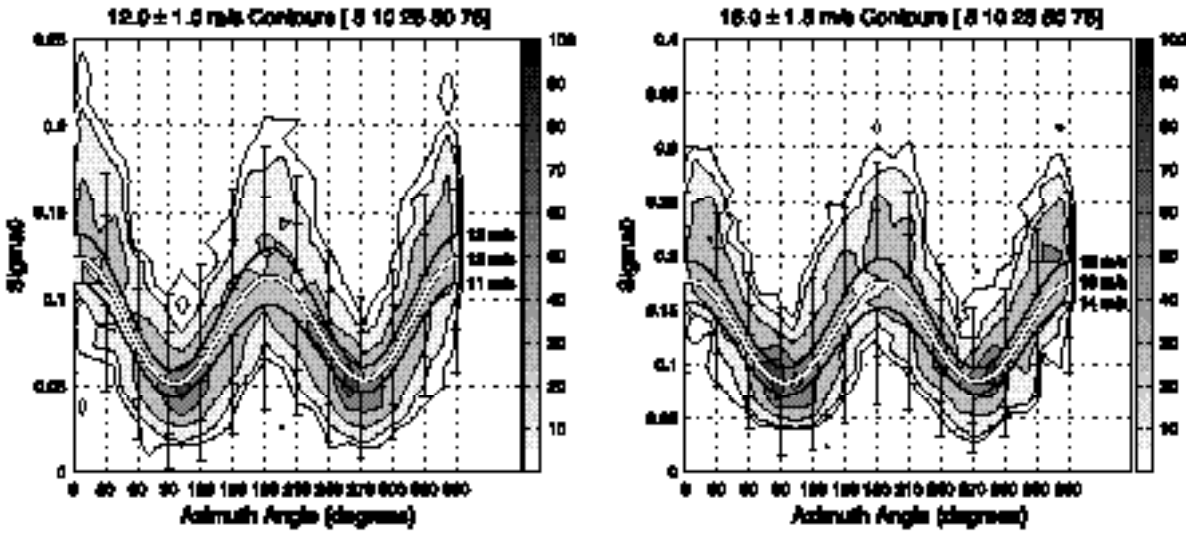

Fig 18 :NN-GMF-V values for different wind speeds (white and black curve) with respect to the azimuth angle for wind speed ranges of $12ms^{-1} \pm 1ms^{-1}$ and $14ms^{-1} \pm 2ms^{-1}$ at an incidence angle of 36.1° against the NSCAT data. In the same figure we plot bars corresponding to one and two standard deviation for some azimuth angles, the standard deviation being derived from NN-VAR results. The darker the shade, the denser the measurements. The scale is given in thousands of points.